Engineering Constraints and Application Regimes of Quantum Radar

Florian Bischeltsrieder, Michael Würth, Johannes Russer *Member, IEEE*, Markus Peichl *Member, IEEE*, and Wolfgang Utschick *Fellow, IEEE*

***Abstract*—Quantum radar is an emerging technique, currently at the experimental stage, that promises to disrupt the well-established field of conventional radar. Recent progress shows that it is possible to generate and use entangled pairs of microwave photons for detection purposes and to obtain an advantage over a classical radar. In this work, we study the currently experimentally feasible type of quantum correlation radar. To this end, we compare different radar architectures, quantum and classical, by analyzing their detection performances by means of the receiver operating characteristic (ROC), the minimum error probability as well as the Chernoff bound. The underlying system models are based on quantum mechanical formulations as well as conventional signal theory. Where it is appropriate and necessary to facilitate our analysis, we apply the central limit theorem to establish the Gaussianity of the observable quantities. A conceptual analogy between the quantum and classic points-of-view is drawn and supported by results showing the asymptotic behavior of the ROC curves of both physical descriptions depending on the power levels of signal and noise. We come to exact and comprehensible conclusions on the current state of quantum radar in comparison to classic radar with a detailed mapping of the radar operating regime (measurement time, signal-to-noise ratio, environmental noise level, target object size and distance) in which a quantum advantage is attainable.**

***Index Terms*—radar, detection, quantum radar, radar theory.**

I. Introduction

The 2023 publication of Assouly et al. entitled *Quantum advantage in microwave quantum radar* may be considered as the first true demonstration of quantum radar using entangled pairs of photons in the microwave regime by, at the same time, showing an advantage over the optimal classic-radar [1]. Previously, there have only been two other notable experiments [2]. One was performed by Luong et al. in 2018 [3], [4], the other by Barzanjeh et al. in 2020 [5].

In the two earlier experiments, the authors were able to generate entangled pairs of microwave photons, however, they relied on non ideal implementations of the transmitter and receiver circuits. An aspect, that is important in classic radar engineering, is the possibility of being able to amplify the transmitted signal. This, however, lead to a problem in the quantum radar experiments. Barzanjeh et al. state in [5] that "[...] the amplified bright noise in the target region overwhelms the environmental noise by orders of magnitude, which precludes the non-invasive character [of quantum radar, F.B.] at short target distances and presents an opportunity to use the presence or absence of the amplifier noise to detect the object [...]." The problem of amplification and it's effect was also discussed in [6], but in the context of quantum communication.

All three experiments demonstrate the current difficulties regarding the technological implementation of a quantum-radar experiment. Additionally, the challenges in setting up a free-space experiment at room temperature are yet to be investigated, as the quantum circuits still require cryostatic conditions with temperatures in the mK-regime.

Despite these challenges, there is a new scientific community emerging connecting quantum physics and conventional radar-engineering. In [7], [8], [9], [10], [11], [12], [13] there are proposals of other implementations of quantum radar compared to Assouly et al. In [14], the possibility of frequency modulation is investigated to enhance range estimations. The authors of [15] describe a quantum-enhanced lidar system for the estimation of velocity. The use of multiple antennas (i.e., arrays) is proposed in [16] and discussed further in [17], [18].

Currently, the most explored type of quantum radar is tailored towards detection purposes. The proposed *quantum illumination* scheme by Seth Loyd in 2008 is about the detection of weak signals in strong noise-backgrounds [19]. In addition, there are already theoretical proposals in this publication of extending the detection technique to ranging or imaging applications [20]. Tan et al. continue in [21] to further analyze the quantum-illumination concept. They propose a quantum-radar concept based on Gaussian states that provides an advantage over any classic-radar scheme. Tan et al. are able to quantify this advantage with a 6 dB gain in the error-exponent for quantum radar compared to classic-radar.

The error-exponent defines a bound on the achievable minimal error probability for detecting correctly the absence or presence of a target. It is widely used in the quantum-radar literature to quantify the achievable gain over a comparable classic radar scheme. The error-exponent is linked to the signal-to-noise ratio (SNR) and the integration time or number of signal samples [2]. However, relying solely on this performance metric instead of analyzing the more commonly used receiver operating characteristic (ROC) in radar engineering has led to severe criticism, as laid out in detail in [22].

In [23], [24], [25], different authors showed that the optimal quantum state saturating Tan et al.'s 6 dB advantage is the

F. Bischeltsrieder and M. Peichl are with the Microwaves and Radar Institute, German Aerospace Center (DLR), 82234 Wessling, Germany (email: florian.bischeltsrieder@dlr.de, markus.peichl@dlr.de).

M. Würth, J. Russer and W. Utschick are with the Chair of Methods of Signal Processing, Technical University of Munich, 80290 Munich, Germany (e-mail: michael.wuerth@tum.de, jrusser@tum.de, utschick@tum.de)

The authors thank the German Federal Ministry for Research and Education (BMBF) for financial support of the investigation on Quantum Radar systems within the QUARATE project.

two-mode squeezed-vacuum (TMSV) state. The corresponding optimal classic counterpart is the coherent state, which is the quantum mechanical description of a sinusoidal signal [19] and is now commonly used for comparison [26]. The TMSV has also been shown to be optimal not only for detection, but also for estimating the transmittance or power loss of a channel [27], [28].

In conventional radar engineering, operating a radar by using a sinusoidal signal is known as the mono-frequency continuous-wave (MF-CW) radar [29] or unmodulated continuous-wave (U-CW) radar [30]. Using this radar type for comparison purposes has again lead to some skepticism in the radar community [22].

To exploit Tan et al.'s full 6 dB quantum advantage, earlier concepts either required the implementation of the signal analysis on a quantum computer [26] or the technique referred to as *feed-forward sum-frequency generation* (FF-SFG) proposed by Zhuang et al. in 2017 [31]. Sorelli et al. note in [2] that the FF-SFG receiver "[...] is extremely complicated and far beyond the capability of state of the art experiments." The scientific significance of Zhuang et al.'s work, however, is undeniable, as this was the first tangible circuit design to fully exploit Tan et al.'s maximal quantum advantage [2]. A more recent development for achieving this optimality is the *correlation-to-displacement* technique proposed by Shi et al. in 2023 [10], [11]. Further explorations of this technique can be found in [12], [32]. Angeletti et al. conclude in [12] that this new approach to quantum radar "significantly reduces the technical challenges associated with optimal receivers, as compared to previous proposals based on [FF-SFG, F.B.]". However, none of the mentioned approaches have been implemented to date.

A more accessible solution was proposed by Guha and Erkmen in [7]. This receiver promises an advantage of 3 dB over a comparable classic radar. Since then, all proposed and experimentally viable quantum radar implementations have promised a quantum advantage of at most 3 dB [1], [3], [4], [5], [9].

For these currently experimentally viable concepts of quantum radar, the measurement protocols are based on the exploitation of strong correlations originating from quantum entanglement. A generator produces a stream of pairs of entangled microwave photons, with each partner photon being separated into one of two parallel signal lines. The currently explored photon-state for this approach is the TMSV as well [2]. The "signal" photons, which are the ones used to illuminate the target, are immersed in thermal noise photons and reduced in number (i.e., signal power) by the scattering that occurs at the target object. The entangled partner photons in the second signal line are stored and accordingly delayed in the quantum-radar system. This photon stream is referred to as "idler". It should be noted that it is also possible to implement the idler without the need for a dedicated signal line with the help of, e.g., a resonator structure [1]. The idler path introduces a time delay matched to the round-trip delay of the measurement path, such that both, signal- and idler-photons, arrive at the receiver at the same time. Here, both photon streams are combined and jointly measured. The operation implemented at the receiver is comparable to a correlation. The output of the receiver is then ready to be measured and recorded [3], [4], [5], [9], [20].

The concept utilized by Luong et al. called *quantum two-mode squeezing* (QTMS) radar is a variation of the before described protocol. The major difference is that the individual signal streams are separately measured instead of performing a joint measurement. This forgoes the use of a matched idler delay [3], [22], [33]. This approach to a experimentally viable quantum radar protocol has as well been discussed by Chang et al. in [34] and referred therein as *quantum-enhanced noise radar*. The QTMS protocol has been criticized in [2] because "[...] when the signal and return mode are measured individually via heterodyne detection it is always possible to find a classical radar that performs as well (sometimes even better) than the quantum one."

Detecting a target using microwave signals in classic engineering is in almost every aspect identical to the described correlation-based quantum radar protocol, except for the utilization of entanglement. It can be summarized as follows [35]: A transmitted signal in the form of an electromagnetic wave propagates into a target area, where a portion of it is scattered back to the radar system depending on the presence or absence of a target object. At the receiver, it is then possible to compare the recorded signal with the transmitted one. When deterministic modulated signals are used, it is possible to do this fully digital. When stochastic signals (i.e., noise) are used, it is required to physically extract and possibly record a copy of the transmitted random-sequence for the successive comparison with the received signal.

Previous publications aimed at a critical analysis of quantum radar. In [36], the authors provide a meta-study like review on quantum radar where they come to a pessimistic conclusions about the usefulness of quantum radar. Different from our work, there is no strict analysis quantifying exact application regions of quantum radar.

A detailed analysis of the aforementioned QTMS radar was carried out by Luong et al., where the authors establish a direct connection to classic noise-type radars [37], [38], [39], [40], [41]. Luong et al.'s innovation over the previous literature is to strictly compare the quantum and classic radar-paradigms using the ROC. Their analysis shows that the QTMS scheme can deliver an advantage over the classic counterpart in terms of the number of signal samples required for computing the correlation coefficient between the signal and idler photons. In addition, Luong et al. make an explicit connection to the, in classic radar engineering well known and frequently used, radar range equation and include device- and environment-specific parameters in their analysis for the QTMS radar. This allows them to draw conclusions about the dependence of the correlation factor on the target distance. A brief summary of the state of the art of quantum radar can be found in [33], and an elaborate discussion is shown in David Luong's dissertation entitled *Quantum Radar Signal Processing* [22].

In [42], Russer et al. analyze the quantum radar scheme of [9] by using the radar range equation to introduce practical modeling parameters (e.g., target cross section and effective antenna area). Wei et al. compare classic and quantum radar using the radar range equation to gain insight into possible

advantages in terms of maximum detection range [43], [44]. Their analysis shows an increased maximal detection range when using quantum radar compared to classic radar under the restriction of a constant transmit power.

The 2023 review articles by Torromé et al. [45] and Karsa et al. [46] provide a comprehensive and detailed overview of the state of quantum radar with an exploration of the currently discussed future prospects and limitations of this technology. The reader is referred to these articles for a current treatment of the history, theoretical foundations and promises of quantum radar. Contrary to these overview publications, we focus on an in-depth analysis specifically on the current experimentally feasible concept of quantum radar exploiting TMSV states with the utilization of a correlation receiver.

The contribution of our research is to provide an engineering- and application-driven analysis of quantum radar. We derive exact and quantifiable conclusions regarding the applicability of the quantum advantage, based on a generalizable methodology that can be applied to future developments as well. We provide a critical analysis of quantum radar from a conventional radar engineering perspective. Based on the assumption of an ideal implementation of quantum radar, we explore operating regimes defined by the signal-to-noise ratio, the noise temperature as well as the frequency and analyze the measurement time necessary for target detection in different scenarios in order to determine extreme cases. Based on these results, we provide a categorization of measurement scenarios regarding their practical feasibility. In addition, we analyze the results of the experiment by Assouly et al. published in 2023 based on the proposed methodology.

The basis of our analysis of quantum radar is a comprehensive yet compact review of the required theory. This includes an overview of the classical signal theoretic description of two classical radar schemes, a quantum mechanical description of classic and quantum radar, and an introduction to detection theory, which is at the core of the currently discussed advantage offered by quantum radar. The detection aspect of radar requires the knowledge of the statistical moments of the desired measurement quantities (i.e., the observables). The first part of this article is concerned with the computation thereof. Note that we apply the central limit theorem to facilitate our derivations and to approximate the observable quantities as being Gaussian distributed in cases where individual statistics are not.

The classically described radar schemes are chosen in analogy to the quantum mechanically described setups. Our aim is to give the classically trained radar engineer a better understanding of the terminology used in quantum mechanics and quantum radar. The reader who is inclined and trained in quantum mechanics may find some insights into classic radar in our presentations, but above all a transparent and clear overview of the quantum mechanical radar model on which our analysis is based. We highlight the conceptual similarities between the different radar concepts and physical points of view by identifying the similarities in the derivation of the statistical parameters relevant for the analysis of the detection performance.

The article is structured as follows. In section II, we provide an overview on the four system concepts discussed in this work, which are described by means of quantum mechanics as well as conventional signal theory. In section III, we briefly lay out the basics of detection theory necessary for the following derivations. We provide an analysis of the dependence of the detection performance of the quantum-mechanical descriptions of the TMSV quantum-radar as well as the coherent-state formulation on the absolute power level. In the concluding analysis of section IV, we explore the applicability of the quantum advantage with respect to scenarios relevant in conventional radar-applications.

II. Radar Concepts

The radar concepts discussed in here are shown as signal-flow diagrams in Fig. 1. The four approaches are, by referring to the labeling of Fig. 1, (a) the coherent-state formulation, (b) the conventional U-CW-radar, (c) the TMSV quantum-radar and (d) a conventional noise-radar. The system models of the TMSV quantum-radar as well as the coherent-state radar are formulated using quantum mechanics. The noise radar as well as the U-CW radar are described by classic signal theory.

The following is an overview of these radar schemes. The detailed derivations and definitions of the quantities introduced herein and used throughout this article are given in the appendix.

Our analysis is done under the assumption of ideal circuit components. The exact details of how specific signal transformations or operations are executed are not of relevance. Note also that all four concepts are phase depended in the sense that perfect knowledge on the distance between target and radar is required. This ensures a matched phase relation (i.e., time delay) between the measurement channel and the idler path or the quadrature detector. This aspect is present in all four radar protocols and will not be discussed in the following analysis, as it is not relevant for the evaluation of the best achievable detection performance.

The U-CW setup's signal flow diagram is illustrated in subplot (b) of Fig. 1. The deterministic transmit signal $s_{\mathrm{T}}(t)$ is directed towards the target. After the noise injection (modeled here as an addition), the radar's receive unit performs a measurement of the quadrature amplitude in-phase with the transmit signal. The observed quantity is X_m, with m enumerating successive samples of the signal.

The noise-radar setup is shown in subplot (d) of Fig. 1. We base our description on [47]. In our approach, however, we do not assume additive noise in the idler path and implement a different quadrature-amplitude correlator, which is in line with the quantum-radar's correlation-operator.

The transmitted measurement signal is $\mathsf{S}_{\mathrm{T}}(t)$ and the retained idler signal is $\mathsf{S}_{\mathrm{I}}(t)$, which are both modeled as random variables and are derived from a common noise source. The target interaction and noise injection is modeled identical to the U-CW description. The measurement signal probes the target, whereas the idler signal is retained and delayed in accordance with the measurement signal's time-delay. At the receiver, samples of the received measurement signal are combined with simultaneous samples of the idler signal in order

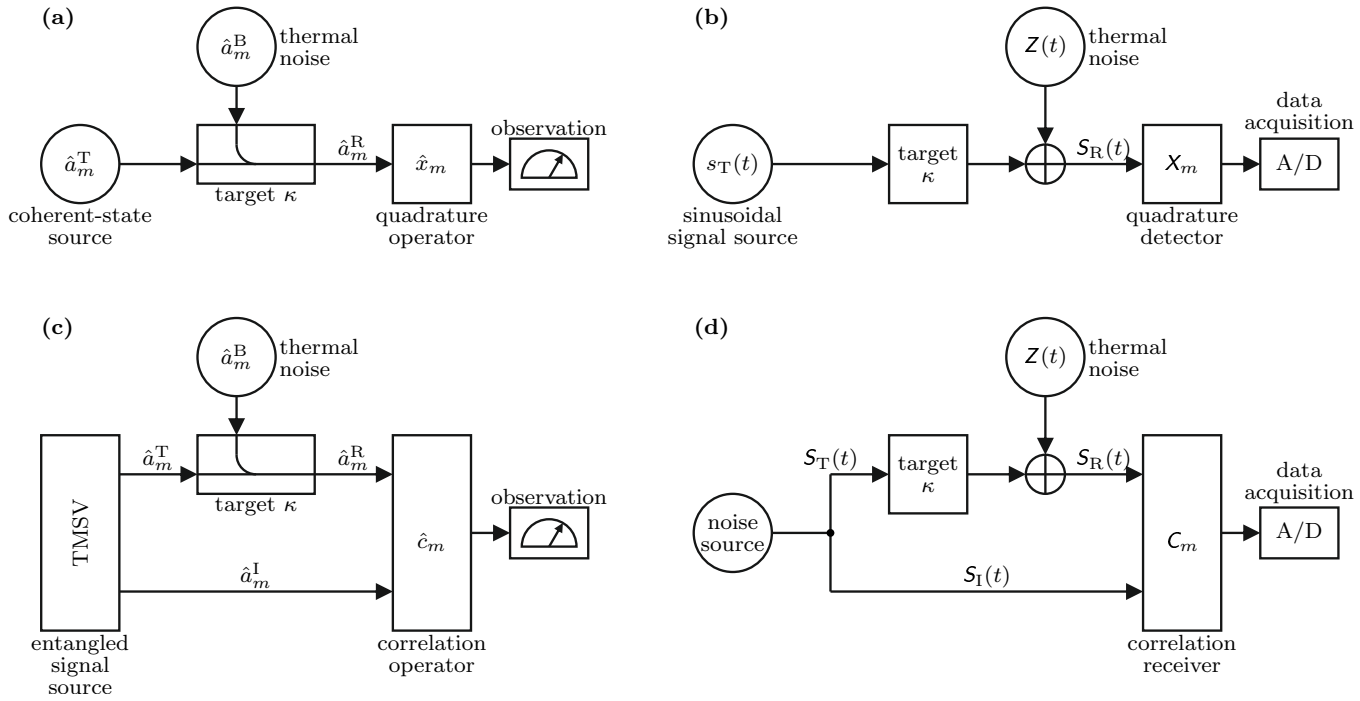

Fig. 1. Overview of different radar approaches as signal-flow diagrams with (a) the coherent-state formulation, (b) the conventional U-CW radar, (c) the TMSV quantum-radar and (d) a conventional noise-radar.

to perform a correlation C_m of their respective quadrature amplitudes.

The signal flow diagram of the coherent state radar is shown in subplot (a) of Fig. 1. The generated probe-signal, subject to the annihilation operator $\hat{a}_m^{\mathrm{T}}$, is directed to a target and measurement scenario modeled as a signal coupler. The combined signal arrives at the radar receiver where a measurement of the quadrature amplitude in-phase with the transmitted signal is performed. The associated measurement operator is $\hat{x}_m$, with m enumerating independent repetitions of the experiment.

In the quantum radar setup (subplot (c) of Fig. 1), a TMSV is generated with the two entangled photons being spatially separated and guided into the measurement and idler signal-paths. The measurement signal probes the target, whereas the idler signal is retained and delayed in accordance with the measurement signal's time-delay. At the receiver, the photons in the signal path are combined with the photons of the idler path in order to perform a pairwise correlation of their quadrature amplitudes, which is described by the operator $\hat{c}_m$.

The four radar schemes discussed in here are in fact only two schemes. However, the mathematical and physical modeling and analysis is done using either purely quantum mechanical considerations or classic signal-theory. Whereas it is possible to establish a strict analogy between the coherent state formulation and the U-CW radar, this strictness does not hold for the comparison of the TMSV quantum radar to the classic noise-radar.

The coherent-state is the quantum-mechanical formulation of the sinusoidal U-CW-signal. The TMSV quantum-radar is only similar to the classic noise-radar with respect to the utilization of correlations. However, in the former approach, quantum correlations are utilized, whereas in the latter case only classic correlations are exploited.

Nevertheless, the transformation of the signals or photons by the propagation through the measurement scene and the scattering at an observed target can be handled in a similar way. Even the correlations, which lie in the quadrature amplitudes of the signals or photons, share a strong similarity. It is only in the last and most crucial computational step, the calculation of the correlation coefficient, that the difference between the capabilities of quantum mechanics and classical signal theory become apparent. The implications of this are subject to the analysis in the following sections.

III. Detection Theory

The detection problem discussed in here can be posed as a hypothesis test with the two alternatives $\mathcal{H}_0$ and $\mathcal{H}_1$, corresponding to the case where there is no target present in the observed measurement scene and the case where there is a target present, respectively. The two hypothesis are quantified using the power loss in the measurement path κ, yielding

$$\begin{aligned} &\mathcal{H}_0 : \text{target absent } (\kappa = 0), \\ \text{and} \quad &\mathcal{H}_1 : \text{target present } (0 < \kappa < 1). \end{aligned} \tag{1}$$

In this section, we present a brief review on the elements of detection theory required for the evaluation of quantum radar, namely the receiver operating characteristic (ROC) and the minimum error probability. We show the behavior of the quantum radar's ROC depending on the operating regime, which is parametrized by the SNR and the noise power.

TABLE I
OVERVIEW OF IMPORTANT PARAMETERS CONCERNING THE DISCUSSED RADAR SCHEMES.
DETAILED DEFINITIONS AND DERIVATIONS ARE SHOWN IN SECTION III AS WELL AS THE APPENDIX.

	moments	SNR	ROC parameters (see (9))
conventional U-CW-radar	$\mu_1 = \sqrt{\kappa} x_\mathrm{T}$ $M\sigma_0^2 = M\sigma_1^2$ $= \sigma_Z^2$	$r = \frac{\kappa x_\mathrm{T}^2}{2\sigma_Z^2}$	$p_1 = 1$ $p_2 = 1$
conventional noise-radar	$\mu_1 = 2\sqrt{\kappa}\sigma_S^2$ $M\sigma_0^2 = 2\sigma_S^2\sigma_Z^2$ $M\sigma_1^2 = 4\kappa\sigma_S^4 + 2\sigma_S^2\sigma_Z^2$	$r = \frac{\kappa\sigma_S^2}{\sigma_Z^2}$	$p_1 = p_2$ $= 1 + 2r$
coherent-state formulation	$\mu_1 = \sqrt{\kappa N_\mathrm{S}}$ $M\sigma_0^2 = M\sigma_1^2$ $= \frac{1}{4}(2N_\mathrm{th} + 1)$	$r = \frac{\kappa N_\mathrm{S}}{N_\mathrm{th}}$	$p_1 = 1$ $p_2 = 1 + \frac{1}{2N_\mathrm{th}}$
TMSV quantum-radar	$\mu_1 = \sqrt{\kappa N_\mathrm{S}(1+N_\mathrm{S})}$ $M\sigma_0^2 = \frac{1}{4} + \frac{1}{4}(2N_\mathrm{th}N_\mathrm{S} + N_\mathrm{th} + N_\mathrm{S})$ $M\sigma_1^2 = \frac{1}{4} + \kappa(N_\mathrm{S} + N_\mathrm{S}^2) + \frac{1}{4}(2N_\mathrm{th}N_\mathrm{S} + N_\mathrm{th} + (1-\kappa)N_\mathrm{S})$	$r = \frac{\kappa N_\mathrm{S}}{N_\mathrm{th}}$	$p_1 = 1 + 4\frac{rN_\mathrm{th} + \frac{3}{4}\kappa}{1 + \frac{\kappa}{r} + \frac{\kappa}{rN_\mathrm{th}} + 2N_\mathrm{th}}$ $p_2 = 2r\left(1 + \frac{1 + \frac{\kappa}{rN_\mathrm{th}} + 2N_\mathrm{th} + \frac{\kappa}{r} - \kappa}{4(rN_\mathrm{th} + \kappa)}\right)$

A. Test statistic

The binary test is based on the test-statistic T defined as

$$\mathsf{T} = \frac{1}{M}\sum_{m=1}^{M} \mathsf{T}_m. \tag{2}$$

Herein, the T_m are representing the outcomes of individual repetitions of an experiment or samples of a signal, with M being the total number of observations.

Depending on the chosen quantum- or classic-radar scheme, we have that

$$\mathsf{T}_m = \begin{cases} \mathsf{X}_m & \text{for the U-CW radar} \\ \mathsf{C}_m & \text{for the noise-radar} \\ \hat{x}_m & \text{for the coherent-state formulation} \\ \hat{c}_m & \text{for the TMSV quantum-radar.} \end{cases} \tag{3}$$

The detailed definitions of the four variants of the statistics T_m can be found in the appendix.

In the following, we discuss the special case of Gaussian-distributed test-statistics T, that are parametrized by the variances σ_0^2 and σ_1^2 as well as the mean μ_1, yielding

$$\mathsf{T} \sim \begin{cases} \mathcal{N}(0, \sigma_0^2) & \text{if } \mathcal{H}_0 \text{ is true} \\ \mathcal{N}(\mu_1, \sigma_1^2) & \text{if } \mathcal{H}_1 \text{ is true.} \end{cases} \tag{4}$$

Note that, for iid T_m and large M, (4) always holds due to the central limit theorem [48].

Since the individual statistics T_m are stochastic independent from each other, it is possible to compute the variances and the mean of T as

$$\mu_1 = \mathrm{E}[\mathsf{T}_m|\mathcal{H}_1], \tag{5}$$

$$\sigma_0^2 = \frac{1}{M}\mathrm{Var}[\mathsf{T}_m|\mathcal{H}_0], \tag{6}$$

$$\text{and} \quad \sigma_1^2 = \frac{1}{M}\mathrm{Var}[\mathsf{T}_m|\mathcal{H}_1]. \tag{7}$$

B. The receiver operating characteristic

The detection performances of the discussed radar-schemes are evaluated by utilizing the ROC given for Gaussian test-statistics with [49] as

$$P_\mathrm{D}(P_\mathrm{FA}) = \Phi\left(\sqrt{\frac{\sigma_0^2}{\sigma_1^2}}\Phi^{-1}(P_\mathrm{FA}) - \sqrt{\frac{\mu_1^2}{\sigma_1^2}}\right) \tag{8}$$

$$= \Phi\left(\sqrt{\frac{1}{p_1}}\Phi^{-1}(P_\mathrm{FA}) - \sqrt{\frac{2Mr}{p_2}}\right). \tag{9}$$

Herein, P_D is the probability of detection and P_FA is the probability of false alarm, $\Phi(\bullet)$ is the complementary cumulative distribution function of a Gaussian distribution with $\Phi^{-1}(\bullet)$ being the respective inverse. Herein, we use a definition of the signal-to-noise ratio r, which is independent of a specific implementation of the radar receiver. The SNR is defined as the ratio of the instantaneously observable powers of the received signal and the environmental noise. Thus, making the SNR agnostic of integration or correlation gains. An overview of all relevant parameters is given in Table I. The detailed derivations are shown in the appendix.

The parameters p_1 and p_2 are introduced to facilitate the following derivations and analysis. They are defined as

$$p_1 = \sigma_1^2/\sigma_0^2, \tag{10}$$

$$\text{and} \quad p_2 = \frac{2Mr}{\mu_1^2/\sigma_1^2}. \tag{11}$$

The parameter p_2 is introduced to make the dependence on the number of samples M as well as the SNR r explicit. Note the ratio Mr/p_2 in (9). With a smaller value p_2, it is possible to reduce Mr without changing the ROC (assuming constant p_1). By keeping Mr and p_1 constant, a reduction of p_2 leads to increased detection probabilities. Thus, smaller values for p_2 are desirable.

It should be noted that Luong et al. provide in [37] a derivation of the PDF of the correlation coefficient of classic noise radar and TMSV quantum radar as well as the ROC of the associated detection problem and hypothesis test (however, for a different implementation of the correlation operator). Contrary to our publication, Luong et al. do not exploit the central limit theorem, but arrive through simulations at the conclusion, that the required PDF is given by a Rice distribution. As the authors state, the Rice distribution converges towards a Gaussian distribution in certain cases. This is, as presented by Luong et al., the case for large sample-numbers M, with which we arrive back at our approach to directly analyze the classic and quantum radar paradigms using the Gaussian assumption.

C. Important limits and transitions

It is known that the performance gain of quantum radar manifests in a regime of high noise-power and low SNR or signal power. As an important prerequisite for our later, more detailed, analysis, and in order to obtain further insights allowing possible simplifications of the otherwise elaborate equations, we show the behavior of the ROC curves of the TMSV quantum radar and the coherent-state formulation in these selected regimes.

The following analysis is carried out with respect to the parameters p_1 and p_2 form (10) and (11), respectively. As introduced in (9), these two parameters fully define the ROCs of all radar concepts considered. The ROCs as well as p_1 and p_2 are formulated such that they depend only on the SNR r, the noise photon number N_{th} and the power loss κ. Hence, it is possible to define an absolute power level by adjusting N_{th}. At the same time, the SNR r can be kept constant, so that the resulting signal power N_{S} is adjusted in concert with the noise power. In the same manner, the SNR can be changed, but keeping the noise power, and therefore the absolute power level, constant.

1) The high-power limit: Our first analysis is concerned with the coherent-state formulation in comparison to the classic U-CW-radar. The relevant parameters defining the ROC are p_1 and p_2. The parameters p_1 of both setups are already identical (see Table I). The parameter p_2 of the coherent state formulation depends only on the parameter N_{th}, so that we are able to compute the high-power limit as

$$\lim_{N_{\text{th}}\to\infty} \{p_2|\text{COH}\} = 1. \tag{12}$$

This result leads to the conclusion that the ROCs for the U-CW radar and coherent state formulation converge towards each other for increasing power-levels.

To investigate the relationship of the TMSV formulation to the classic noise-radar, we show the convergence of both parameters, p_1 and p_2. For the classic scheme, we have identical parameters with $p_1 = p_2$.

First, we consider p_1 of the TMSV formulation. By increasing the noise power, we get

$$\lim_{N_{\text{th}}\to\infty} \{p_1|\text{TMSV}\} = 1 + 2r. \tag{13}$$

In the next step, we analyze p_2 and get

$$\lim_{N_{\text{th}}\to\infty} \{p_2|\text{TMSV}\} = 1 + 2r. \tag{14}$$

Both ROC parameters converge to the results obtained for the classic noise-radar. Even though effects such as entanglement are not obtainable using the capabilities of conventional radar-technology, the detection performances of both paradigms nevertheless converge.

This result does not contradict the established theory, as this limit analysis is done in a parameter regime with high noise-power and a finite SNR (i.e., high signal-power). The quantum advantage, as it was discussed in [50], for instance, manifests in high noise-power and low signal-power regimes.

2) The low SNR regime: The ROC parameters of the coherent-state formulation do not depend on the SNR, whereas p_1 and p_2 of the TMSV quantum radar do. The low SNR limit of p_1 yields

$$\lim_{r\to 0} \{p_1|\text{TMSV}\} = 1, \tag{15}$$

which indicates that the variances σ_0^2 and σ_1^2 of the two alternative hypothesis are identical in the low SNR regime. We are going to exploit this circumstance throughout the following analyses.

The limit for p_2 and the TMSV quantum radar is

$$\lim_{r\to 0} \{p_2|\text{TMSV}\} = \frac{1}{2}\left(1 + \frac{1}{N_{\text{th}}}\right). \tag{16}$$

This result permits already at this point to conclude for a quantum advantage, as the parameter p_2 converges towards 1/2 in a second limit computed for $N_{\text{th}} \to \infty$. In contrast, the parameters of the other radar concepts are identical to one in the same limits. A detailed discussion of the quantum advantage follows in the next chapter.

D. ROC and error probability

The ROC curve for a maximum-likelihood test based on a Gaussian test-statistic T is given by (9). From (15) we know that $p_1 \approx 1$ holds in the parameter regime relevant for quantum radar. In the following, we thus consider only ROC curves of the type

$$P_{\text{D}}(P_{\text{FA}};\chi) = \Phi\big(\Phi^{-1}(P_{\text{FA}}) - \sqrt{\chi}\big), \tag{17}$$

which is a function of the false-alarm probability and parametrized by $\chi = \mu_1^2/\sigma_1^2 = 2Mr/p_2$.

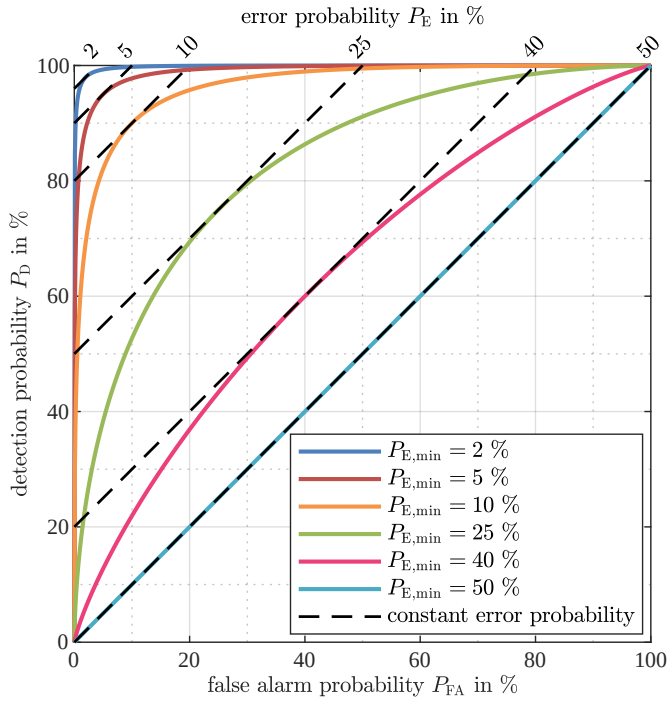

Fig. 2. ROC curves of type (17) for selected minimum error probabilities (equally probable hypothesis $\mathcal{H}_0$ and $\mathcal{H}_1$; see (20), (21)).

The performance of a detector can be quantified, among other metrics, by the minimum achievable error-probability $P_{\mathrm{E,min}}$. The error probability P_{E}, by assuming equally-probable hypothesis, yields [51]

$$P_{\mathrm{E}} = \frac{1}{2}(P_{\mathrm{FA}} + (1 - P_{\mathrm{D}})). \tag{18}$$

With the help of the ROC we get

$$P_{\mathrm{E,min}} = \frac{1}{2}\left(1 + \min_{P_{\mathrm{FA}}\in[0,1]} \{P_{\mathrm{FA}} - P_{\mathrm{D}}(P_{\mathrm{FA}})\}\right). \tag{19}$$

From [49] it is known that in the case of equally probable hypothesis $\mathcal{H}_0$ and $\mathcal{H}_1$ we have

$$P_{\mathrm{E,min}} = \Phi\left(\frac{1}{2}\sqrt{\chi}\right) \quad \leftrightarrow \quad \sqrt{\chi} = 2\Phi^{-1}(P_{\mathrm{E,min}}). \tag{20}$$

Hence, the parameter χ can be used interchangeably with the minimum error probability $P_{\mathrm{E,min}}$, resulting in

$$P_{\mathrm{D}}(P_{\mathrm{FA}}; P_{\mathrm{E,min}}) = \Phi\big(\Phi^{-1}(P_{\mathrm{FA}}) - 2\Phi^{-1}(P_{\mathrm{E,min}})\big). \tag{21}$$

This result shows that $P_{\mathrm{E,min}}$ can be used as the single parameter defining the entire ROC. For cases in which the prior-probabilities of the two alternative hypothesis are identical, the parameter $P_{\mathrm{E,min}}$ has an actual meaning, i.e., it is truly the minimal error probability. In other situations with arbitrary prior probabilities, the shown $P_{\mathrm{E,min}}$ has no direct interpretation, other then being the parameter defining the ROC.

Fig. 2 contains ROC curves for different choices of $P_{\mathrm{E,min}}$, with which it is possible to relate ROC curves directly to the minimum error probability. In the remainder of this article, we thus restrict our discussion and analysis to $P_{\mathrm{E,min}}$ as our figure of merit. Fig. 2 should enable the reader to reference our later statements with respect to $P_{\mathrm{E,min}}$ to the corresponding ROC curve.

It should be noted that not in every detection scenario is the assumption of equally probable hypothesis correct, and neither do universally hard limits on the required minimal probability of detection and false-alarm probability exist. These choices depend on the operator and the application. To relate the ROC curves to the minimal error probability, as done in here, enables general conclusions and incorporates various applications, because the ROC curves displayed in Fig. 2 are not tied to specific values of κ, M or r, for instance.

We hope that our approach can help to bridge the different established viewpoints in the literature on quantum radar, in which the error probability and bounds thereof are used as a performance metric, and classic radar, where the ROC is considered as the standard for thorough and comprehensive analyses.

IV. The Quantum Advantage

In the following, we define the quantum advantage in accordance with the quantum-radar literature using the Chernoff bound. We provide an analysis of the limits of the quantum advantage and derive a formula to compute the maximally achievable quantum-advantage.

A. Definition

The quantum advantage is typically defined by means of the Chernoff bound on the error probability P_{E} of making a wrong decision with respect to the discussed two-hypothesis test. By assuming that both hypothesis are equally probable, it follows that

$$P_{\mathrm{E}} \leq \frac{1}{2} \min_{\alpha\in(0,1)} \exp\{-C_\alpha\}, \tag{22}$$

with the Chernoff α-divergence C_α depending on the optimization parameter α [52]. Note that the dependence on the number of samples M is implicitly included in this formulation of the Chernoff bound compared to explicit formulations as introduced in [2], for instance. This is due to the introduction of the test statistic T in (2) as the M-sample mean.

The potential gain in detection performance offered by quantum radar is thus defined using the optimal C_α for the cases of the TMSV quantum-radar and the coherent-state formulation as

$$Q_{\mathrm{A}} = \frac{\max_{\alpha\in(0,1)} \{C_\alpha | \,\mathrm{TMSV}\}}{\max_{\alpha\in(0,1)} \{C_\alpha | \,\mathrm{COH}\}}. \tag{23}$$

We discuss the case shown in (4), i.e., a Gaussian distributed test-statistic with $\mathrm{E}[T|\mathcal{H}_0] = 0$. The Chernoff α-divergence results, referring to [52], in

$$\begin{aligned} C_\alpha = &\frac{1}{2}\log\left(\frac{\alpha\sigma_0^2 + (1-\alpha)\sigma_1^2}{(\sigma_0^2)^\alpha(\sigma_1^2)^{(1-\alpha)}}\right) + \\ &\frac{\alpha(1-\alpha)}{2}\frac{\mu_1^2}{\alpha\sigma_0^2 + (1-\alpha)\sigma_1^2}. \end{aligned} \tag{24}$$

By assuming that $\sigma_0^2 \approx \sigma_1^2$ (i.e., $p_1 \approx 1$), we get

$$C_\alpha \approx \frac{\alpha(1-\alpha)}{2}\frac{\mu_1^2}{\sigma_1^2}. \tag{25}$$

From (25) and (22) it follows that the optimal $\alpha = 1/2$, which is independent of μ_1^2/σ_1^2. This allows to directly compare the Chernoff α-divergences of different measurement schemes. With (25) and (11) we get

$$Q_{\mathrm{A}} \approx \frac{\left(\mu_1^2/\sigma_1^2\right)|\,\mathrm{TMSV}}{(\mu_1^2/\sigma_1^2)|\,\mathrm{COH}} \tag{26}$$

$$= \frac{p_2|\mathrm{COH}}{p_2|\mathrm{TMSV}}. \tag{27}$$

Thus, we obtain the quantum advantage with the parameters p_2 given in Table I as

$$Q_{\mathrm{A}} = \frac{1+\dfrac{1}{2N_{\mathrm{th}}}}{2r\left(1+\dfrac{1+\dfrac{\kappa}{rN_{\mathrm{th}}}+2N_{\mathrm{th}}+\dfrac{\kappa}{r}-\kappa}{4(rN_{\mathrm{th}}+\kappa)}\right)}. \tag{28}$$

B. Interpretation and limit analysis

From [26] we already know that the quantum advantage manifests for high thermal-noise backgrounds with low signal-power-levels. To this end, we introduce the auxiliary variables n_{S} and n_{th} together with the adjustable parameter Ω, with which we define

$$N_{\mathrm{S}} = \frac{n_{\mathrm{S}}}{\Omega}, \tag{29}$$

$$N_{\mathrm{th}} = \Omega n_{\mathrm{th}}, \tag{30}$$

$$\text{and} \qquad r = \frac{\kappa n_{\mathrm{S}}}{\Omega^2 n_{\mathrm{th}}}. \tag{31}$$

With these reformulations, we are able to achieve the desired power-level adjustments simultaneously by increasing Ω. Thus, the quantum advantage Q_{A} from (28) is in the following dependent on Ω, viz. $Q_{\mathrm{A}} = Q_{\mathrm{A}}(\Omega)$.

We increase Ω and obtain

$$\lim_{\Omega\to\infty} Q_{\mathrm{A}}(\Omega) = 2. \tag{32}$$

This result is in accordance with the already known result that the utilization of quantum entanglement may deliver an advantage of a factor of 2 [7].

The quantum advantage is introduced with respect to the error exponent and the corresponding minimal error probability. It is, by referring to (27), equally possible to interpret the quantum advantage as a factor quantifying the improvement of the ROC, since it depends directly on p_2 (see (9)). In consequence, it is possible to translate the quantum advantage of an improved detection performance as well to an advantage of the resources SNR or sample number. A different approach to the potential reduction of the required number of samples can be found in [38], [53], for instance.

C. Noise threshold

In the following, those power-regimes are investigated, for which a quantum advantage can be expected. We rearrange (28) such that the explicit dependence of the SNR on the noise-photon number is obtained. The result can bee seen in (33). The resulting equation has two solutions, of which we only consider r_+. The neglected solution r_- has no physical relevance.

We analyze r_+ in the low-SNR regime. By setting (33) to zero, we obtain one zero-crossing for the noise photon-number N_{thr} at

$$N_{\mathrm{thr}} = \frac{Q_{\mathrm{A}}-1}{2-Q_{\mathrm{A}}}. \tag{34}$$

Since photon numbers are positive values, we have to require that $Q_{\mathrm{A}} > 1$. This is in accordance with the result that the TMSV quantum-radar should not be outperformed by a coherent-state radar in the discussed low SNR regimes.

Let us now discuss whether N_{thr} limits the possible noise photon numbers for a targeted quantum-advantage from below or above. To this end, we compute the gradient of r_+ with respect to N_{th} at the discussed zero crossing. We get

$$\left.\frac{\partial r_+}{\partial N_{\mathrm{th}}}\right|_{N_{\mathrm{th}}=N_{\mathrm{thr}}} = \frac{\overbrace{\kappa(Q_{\mathrm{A}}-2)^3}^{<0}}{\underbrace{\left(Q_{\mathrm{A}}^2-Q_{\mathrm{A}}\right)}_{>0}\underbrace{\left(\underbrace{1-Q_{\mathrm{A}}}_{<0}+\underbrace{3\kappa(Q_{\mathrm{A}}-2)}_{<0}\right)}_{<0}} > 0, \tag{35}$$

which leads, together with $Q_{\mathrm{A}} \in (1,2)$, to the conclusion that the gradient is positive at the zero crossing and that the noise photon number is lower bounded by N_{thr}.

In order to achieve a certain quantum-advantage, it is therefore required to have a minimum noise-floor. The common knowledge of classic radar-engineering that lower noise levels are always desirable, does not hold with respect to the quantum advantage.

D. Maximum achievable quantum advantage

By reformulating (34) as a function of Q_{A} depending on the noise photon-number, we are able to obtain an upper bound $Q_{\mathrm{A,max}}$ on the possible quantum advantage. We get

$$Q_{\mathrm{A,max}} = 2 - \frac{1}{1+N_{\mathrm{th}}}. \tag{36}$$

Fig. 3 shows the maximum achievable quantum advantage depending on T/f instead of the photon number (the relation between these quantities is given by (76)). The choice to use the ratio of the noise temperature T to the signal frequency f in units of K/GHz for the horizontal axis is due to practical reasons. The use of photon numbers or rates is not common in radar engineering. With the chosen scaling, it is directly possible to convert the axis to a noise-temperature axis by choosing a specific signal-frequency, which are most commonly found in the GHz regime when discussing radar applications. The

$$r_{\pm} = \frac{2N_{\text{th}} + 1 - Q_{\text{A}}(3\kappa + 2N_{\text{th}} + 1) \pm \sqrt{(3Q_{\text{A}}\kappa + 2(Q_{\text{A}} - 1)N_{\text{th}} + Q_{\text{A}} - 1)^2 - 16Q_{\text{A}}\kappa((Q_{\text{A}} - 2)N_{\text{th}} + Q_{\text{A}} - 1)}}{8Q_{\text{A}}N_{\text{th}}} \tag{33}$$

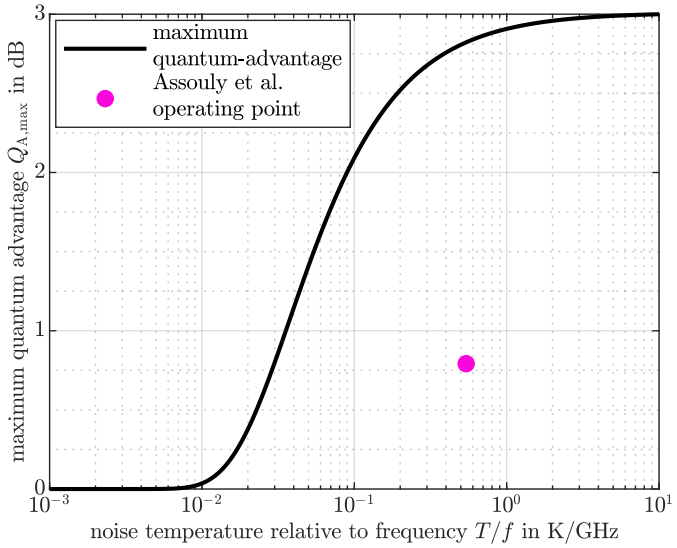

Fig. 3. Maximum possible quantum advantage. Note that a similar depiction, however for a different case with 6 dB maximal quantum advantage, is shown in [6].

noise temperature is again a comprehensible quantity that is used and understood in radar engineering.

We see that for $T/f < 10^{-2}$ K/GHz, the quantum advantage is approximately 0 dB. Desirable quantum advantages with $Q_{\text{A}} > 2$ dB are achievable only for $T/f > 10^{-1}$ K/GHz.

Most long-range radar-applications operate in the frequency regime up to 10 GHz [54]. To simplify our analysis, we use $f \in [1, 10]$ GHz. We assume typical temperatures ranging from $T \approx 5$ K (cosmic microwave-background observable from the earth's surface) [55] to $T \approx 293$ K$\hat{=}$20° C (typical room-temperature). With these limits, we get $T/f \in \left[5 \cdot 10^{-1}, 293\right]$ K/GHz $\Rightarrow$ $Q_{\text{A,max}} \in [2.8, 3]$ dB. This analysis shows that, in principle, it should be possible to implement a quantum radar that achieves a desirable quantum-advantage in typical long-range scenarios.

We mark the operating point of the experiment by Assouly et al. [1] in Fig. 3. With a stated noise photon number of $N_{\text{th}} = 10.8$ we arrive with (76) at $T/f = 0.542$ K/GHz. The quantum advantage is given as $Q_{\text{A}} = 1.2\hat{=}0.79$ dB. With (36) we obtain a maximally achievable quantum-advantage of $Q_{\text{A,max}} = 1.92\hat{=}2.82$ dB for the experiment conditions of Assouly et al. Consequently, there is a gap of approximately 2 dB between the realized quantum-advantage and the achievable quantum-advantage.

V. The Applicability of the Quantum Advantage

With the previous results, it is possible to analyze scenarios relevant in radar remote-sensing with respect to the applicability and usefulness of a quantum radar providing a quantum advantage.

We begin by selecting relevant scenarios based on the power loss κ and extract operating points parametrized by the SNR r and the ratio T/f. We use these parametrized scenarios to estimate the approximate measurement-time for the quantum radar and to obtain bounds on the permissible power-loss. Finally, we provide a method to select scenarios where the deployment of quantum radar might be beneficial.

A. Power and Environmental Limitations

Fig. 4 illustrates r_+ from (33) as a function of T/f for a quantum advantage of 2 dB$\hat{\approx}$1.6 and 3 dB$\hat{\approx}$2. We have chosen four different scenarios that are quantified by the total power-loss in the measurement path: $\kappa \in \{-10, -50, -80, -180\}$ dB. The values are not chosen arbitrarily, but in conjunction with the analysis that follows in the subsequent sections.

The exemplary curves in Fig. 4 show the before analyzed lower bounds on N_{th}, which translate here to lower bounds on the ratio T/f. In more detail, the graphs show that, in order to achieve a specific quantum advantage, it is necessary to adjust the SNR opposite to a decrease or increase of the noise power. Even though it is necessary to provide a certain minimal noise-floor, it is nevertheless advantageous to adjust the quantum radar, such that a low T/f-value is obtained. As long as the discussed threshold is not broken, it is possible to optimize the measurement setup with respect to a maximally possible SNR.

Fig. 4 includes reference lines (plotted in black) at selected values of T/f. By choosing room temperature noise, we obtain the frequencies written to these lines. It follows that, in order to obtain a certain quantum advantage at a specific temperature, the signal frequencies are upper bounded. The upper bounds at room temperature are approximately 3274 GHz and 29 GHz for a 2 dB or 3 dB quantum advantage, respectively. We may safely assume that most long-range radar applications operate at frequencies that are well below these values, which indicates that there might be the possibility to benefit from quantum technology in such applications.

If we target an operating point that allows us to exploit the highest possible SNR for a given quantum advantage, we have to choose a specific signal frequency. At room temperature, the maximal SNR values are attainable only with approximately 1707 GHz and 13 GHz for a 2 dB or 3 dB quantum advantage, respectively. Of these two frequencies, only the latter is within a range that may be usable for radar applications. However, this frequency may already be to high for some long-range scenarios.

We indicate the operating point of Assouly et al. in Fig. 4. With the SNR defined by (86) and $\kappa = 3.02 \cdot 10^{-2}\hat{=}-15.2$ dB, $N_{\text{S}} = 3.53 \cdot 10^{-2}$ and $N_{\text{th}} = 10.8$ from [1] we calculate a SNR of $r = 9.87 \cdot 10^{-5}\hat{=}-40.1$ dB. Additionally, we include

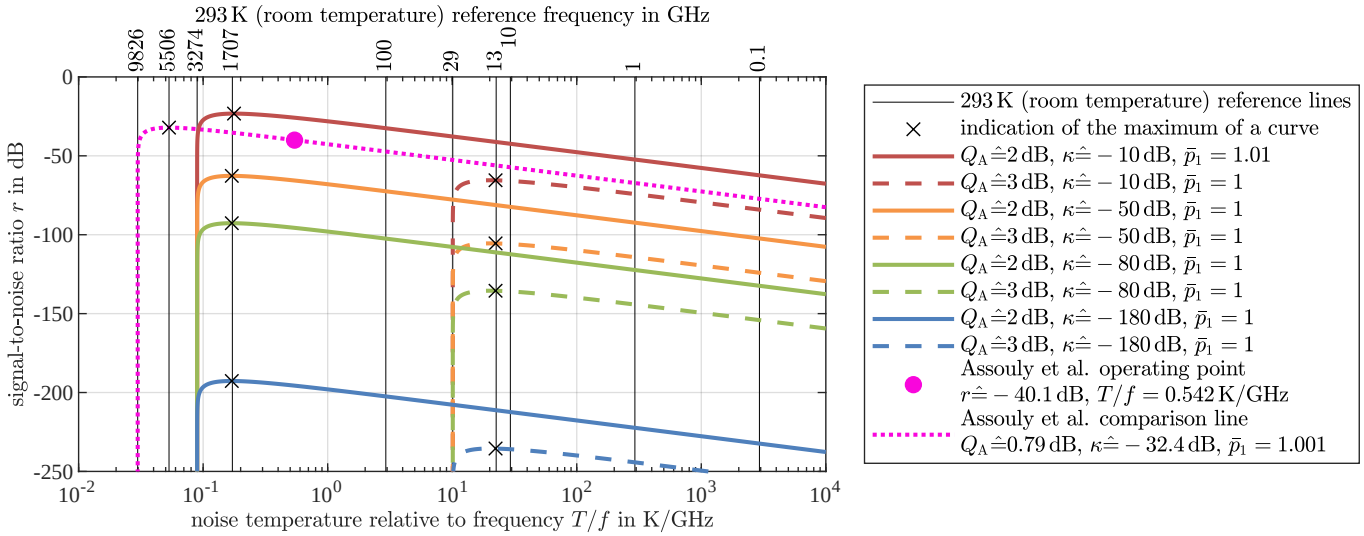

Fig. 4. Illustration of the 2 dB and 3 dB quantum advantage for different scenarios parametrized by the total power loss κ in the measurement path. The values $\bar{p}_1$ are the observed maximal values of p_1 for each shown curve, thus justifying the assumptions leading to (25).

a comparison line for the SNR depending on T/f (see (33)) for the Assouly et al. experiment conditions, where we adjust the power loss, such that the comparison line coincides with the reference point.

The necessary power loss to achieve this coincidence is determined by us to be approximately $\kappa \hat{=} -32.4\,\text{dB}$. We see that the Assouly et al. quantum radar achieves the same performance as would an ideal quantum-radar that operates on a measurement channel with a power loss that is increased by 17.2 dB.

The final aspect that shall be discussed with respect to Fig. 4 is the relation between the maximally possible SNR and the desired quantum advantage. By observing the maximal SNR of the 2 dB quantum advantage curves, we find that the SNR is approximately 13 dB bellow the power loss κ of the corresponding curves. Consequently, the transmitted signal power has to be 13 dB below the thermal-background's noise-power. The same analysis can be done for the 3 dB quantum advantage curves. Here we find that the transmitted signal power has to be approximately 55 dB below the thermal-background's noise-power.

In order to achieve just 1 dB more quantum advantage, the SNR has to be reduced by approximately 42 dB. Additionally, the signal frequency has to be changed as well, if we assume that the noise temperature remains constant.

B. Detection Performance and Measurement Time Expense

In the following, we discuss $P_{\text{E,min}}$ in dependence on the number of samples (or experiment repetitions) M for four different sets of parametrizations, namely, power loss κ, SNR r and relative temperature T/f.

We expect that, by increasing the number of utilized samples, the minimum error-probability should decrease. An error probability of 50 % may be considered a fully random detection outcome, comparable to a coin-toss.

For our analysis, we assume that already error probabilities below 25 % may be considered desireable. Note that this limit is meant as an absolute tolerable bound on the ROC (see Fig. 2). In most practical applications, we may safely assume that such an ROC would not be of much use. However, as we are going to see in the following, the measurement time expenses needed for improved ROC curves are in the same order of magnitude as for this extreme edge case.

1) Maximal experiment repetition frequency: In [41], the authors provide a first rough analysis of the expected measurement-time in one specific radar-scenario by using a sampling-frequency of 1 MHz for their computation. This value, however, is not supported by further explanations.

To evaluate the measurement-time expense, we approximate the measurement time assuming that the signal-samples are recorded successively with a constant repetition frequency f_S. The total measurement time T_{tot} is then

$$T_{\text{tot}} = \frac{M}{f_S}. \tag{37}$$

The exact value of f_S depends highly on the hardware implementation as well as the technological maturity of quantum radar. In the following, we provide a favorable guess for the sampling frequency.

As a general rule, we require that the time between two successive measurements is chosen such that the samples are stochastically independent. This ensures that the experimentally obtained samples are in line with the assumptions that allow to formulate the ROC as (9) and the moments as (5), (6) and (7). Consequently, the sampling interval has to be greater than the maximum time-extend of any frequency-limiting device's impulse response (e.g., filters or resonators). Thus, the sampling frequency needs to be less then the respective minimal bandwidth Δf_{min}, such that

$$\frac{1}{f_S} > \frac{1}{\Delta f_{\text{min}}} \quad \leftrightarrow \quad f_S < \Delta f_{\text{min}}. \tag{38}$$

Another limiting factor might be due to the availability of fast analog-to-digital converters. Modern devices based

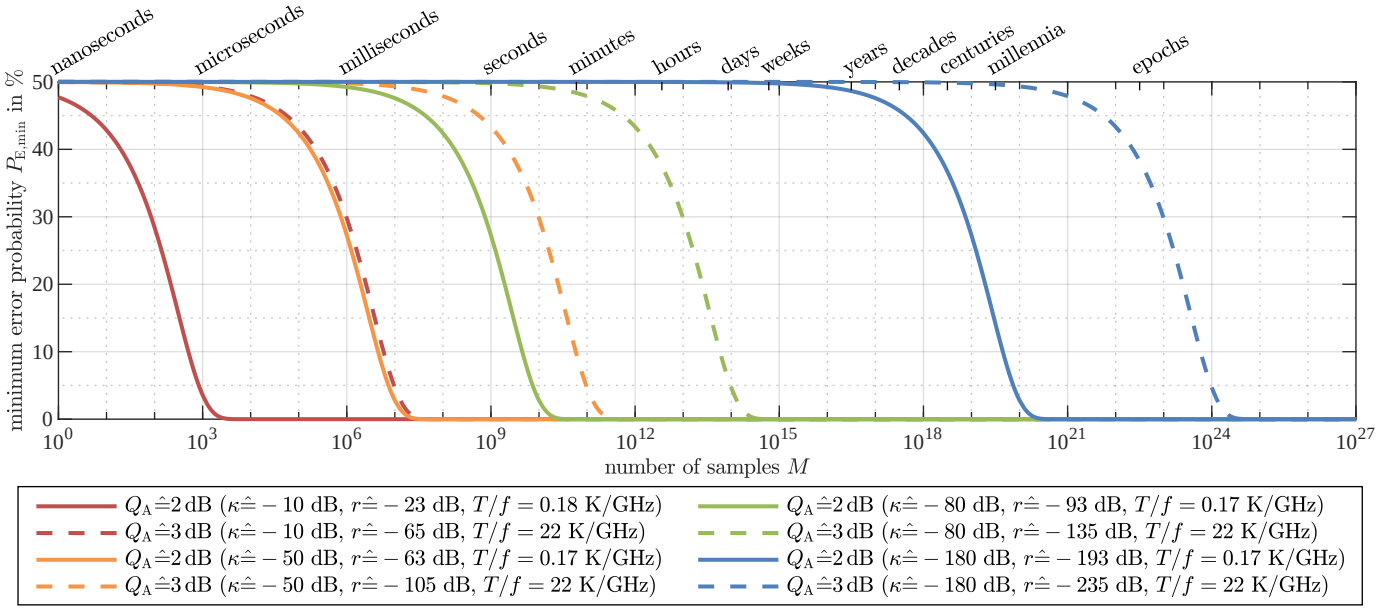

Fig. 5. Minimum error probability as a function of the number of samples (or experiment repetitions) for a quantum advantages of 2 dB and 3 dB and the same power loss values κ as seen in Fig. 4. The measurement time is computed by assuming a sampling frequency of $f_\mathrm{S} = 1\,\mathrm{GHz}$. Note that the minimal error probabilities can be related to specific ROC curves using Fig. 2.

on field programmable gate array (FPGA) technology offer sampling frequencies of up to 5 GHz [56], whereas some oscilloscopes reach up to 40 GHz [57], for instance. As we are going to show in the following, key components are designed with extremely small bandwidths. Hence, the ultimate time-limiting factor is not given by the sampling frequency of available analog-to-digital converters.

With the current technological implementations of quantum radar, we may assume that the lowest bandwidths are given by the resonating structures of the Josephson amplifiers. With the help of the resonator quality-factor Q, we get [58]

$$\Delta f_\mathrm{min} = \frac{f}{Q}. \tag{39}$$

From [59] we know that values of $Q > 10^4$ are desired for quantum applications. We assume that reasonable values of the quality factor are $Q \in \left[10^4, 10^5\right]$ for signal frequencies $f \in [1, 10]\,\mathrm{GHz}$. With (38) and (39) we get $\Delta f_\mathrm{min} \in [0.01, 1]\,\mathrm{MHz}$.

It follows that the sampling frequency is limited to $f_\mathrm{S} < 0.01\,\mathrm{MHz} \ldots 1\,\mathrm{MHz}$, depending on the details of the hardware implementation.

In order to accommodate for technological advancements and circumstances that have not been considered here, we use an exemplary sampling-frequency of $f_\mathrm{S} = 1\,\mathrm{GHz}$, which is three orders of magnitude larger then the maximal value obtained from our rough computation.

2) Analysis and discussion: Fig. 5 illustrates the expected minimal error probabilities depending on the number of samples. The estimated measurement times range from the nanoseconds regime ($\kappa\hat{=}-10\,\mathrm{dB}$) to several centuries ($\kappa\hat{=}-180\,\mathrm{dB}$). We assume that for practical applications, the measurement time should be at maximum in the range of several seconds or, to be more realistic, in the range of several milliseconds.

Furthermore, we assume that, due to implementation details, the utilized quantum advantage is chosen to be 2 dB. With a maximally permissible error probability of 25 %, we arrive at the conclusion that we can allow for a total measurement path power loss of at maximum $-80\,\mathrm{dB}$, but more realistically we should limit the power loss to $-50\,\mathrm{dB}$.

As stated in the beginning of this section, the chosen error probability of 25 % poses an extreme case. In Fig. 5 we see that, for the before chosen reference curves, the measurement time durations resulting in improved ROC curves with lower minimal error probabilities lie in the same order of magnitude as the previously determined time-scales.

C. Possible Radar Scenarios

In the previous analyses, we determined the maximally permissible power-loss in a general measurement scenario. In the following, we determine the specific radar scenarios, in which we can expect to benefit from quantum radar technology. We characterize a scenario by the distance between the radar's antennas and the target object as well as the size of the target.

The first characteristic is used, because the distance introduces an additional signal power loss due to the nature of the wave propagation. The object size is chosen over the more accurate parameter radar cross section (RCS), as this quantity is independent of the frequency or object shape and can therefore be applied more generally, especially to obtain a first rough guess, whether a specific target can be detected or not.

1) Maximum power loss and minimal object size: The total power loss κ is computed using the radar range equation [60].

With the RCS σ, the distance d, the antenna gain G and the vacuum speed of light c_0 we have

$$\kappa = \frac{G^2 \mathrm{c}_0^2 \sigma}{(4\pi)^3 d^4 f^2}. \tag{40}$$

Note that we assume the applicability of the classical concepts of RCS and antenna gain in the context of quantum radar.

In order to obtain an estimate for the detectable object-size, we make the following argument: a triangular corner reflector (TCR) is often used as an almost ideal retro-reflector. In good approximation, we assume that any target, that is of the same size as the TCR, delivers less reflected signal power then the TCR. When we assume that the RCS of any target increases with size, then it is possible to bound the detectable object-size by the size of the TCR.

The RCS σ_{TCR} of a TCR of size a_{TCR} is given as [54]

$$\sigma_{\mathrm{TCR}} = \frac{4\pi a_{\mathrm{TCR}}^4 f^2}{3\mathrm{c}_0^2}. \tag{41}$$

With (41) and the radar range equation (40) we get

$$\kappa_{\mathrm{TCR}} = \frac{G^2}{3(4\pi)^2}\Big(\frac{a_{\mathrm{TCR}}}{d}\Big)^4 \tag{42}$$

for the TCR's power loss κ_{TCR}. The necessary size of a TCR for a given power loss, antenna gain and target distance yields

$$a_{\mathrm{TCR}} = d\left(\frac{3(4\pi)^2 \kappa_{\mathrm{TCR}}}{G^2}\right)^{1/4}. \tag{43}$$

From (43) and (42) it follows that the TCR size and the TCR power-loss are independent of the frequency. This is beneficial for the following analyses, as it allows us to formulate general conclusions regarding the applicability of quantum radar.

With the previously made argumentation, we are now able to formulate bounds on the expected power loss and the necessary target size as

$$a(\kappa, d) > a_{\mathrm{TCR}}(\kappa, d) \quad \text{and} \quad \kappa(d/a) < \kappa_{\mathrm{TCR}}(d/a). \tag{44}$$

2) Antenna gain: A major influence on the power budget of a radar measurement setup is due to the antenna gain G. In order to base the following analysis on meaningful values, we bound the antenna gain for general radar scenarios.

To this end, we make the argument that the object size a has to be less then the extend A of the area illuminated by the radar's antenna, viz.

$$a < A. \tag{45}$$

With the formula given in [61], it is possible to approximate the antenna gain as

$$G \approx e_{\mathrm{r}} \frac{\rho_{\mathrm{DBP}}}{\Delta\varphi_{\mathrm{E}} \Delta\varphi_{\mathrm{H}}}, \tag{46}$$

where e_{r} is the radiation efficiency, ρ_{DBP} is the directivity-beamwidth-product and $\Delta\varphi_{\mathrm{E}}$ and $\Delta\varphi_{\mathrm{H}}$ are the beam-width angles measured in orthogonal radiation-planes.

By assuming that $\Delta\varphi_{\mathrm{E}} = \Delta\varphi_{\mathrm{H}}$ in (46), we get

$$A \approx \frac{d}{F}, \tag{47}$$

with the factor F yielding

$$F = \frac{1}{2}\cot\left(\sqrt{\frac{\rho_{\mathrm{DBP}}}{4G}}\right). \tag{48}$$

We require that the target object size should be limited to $a \leq d/10$. This requirement is due to practical reasons, as we do not expect object dimensions to be in the same order of magnitude as the target distance for relevant detection scenarios. In order to fully illuminate the largest permissible objects, we get with (45) the requirement

$$F \leq 10. \tag{49}$$

If we assume loss-less antennas (i.e., $e_{\mathrm{r}} \approx 1$) and use $\rho_{\mathrm{DBP}} \approx 26 \cdot 10^3 \cdot (1^\circ)^2$ (see [61]), we obtain:

$$\begin{aligned} G \hat{=} 10\,\mathrm{dBi} &\Rightarrow F \approx 1, \\ G \hat{=} 20\,\mathrm{dBi} &\Rightarrow F \approx 3.5, \\ G \hat{=} 30\,\mathrm{dBi} &\Rightarrow F \approx 11, \\ \text{and} \quad G \hat{=} 40\,\mathrm{dBi} &\Rightarrow F \approx 35.5\,. \end{aligned}$$

Antennas with a gain of $40\,\mathrm{dBi}$ result in F-values that are above the derived limit, whereas antennas with a gain of $10\,\mathrm{dBi}$ are illuminating an unpractical large area that is of the same extend as the targeted distance. In the following, we consider $G \in \{20, 30\}\,\mathrm{dBi}$ for our analysis. The lower of the two gain-values is in good approximation a viable candidate for the monitoring of a large area. The larger value might be considered for the precise monitoring of a narrow areal.

3) Scenario analysis and discussion: The result of the presented analysis can be seen in Fig. 6. The two shown illustrations contain complementary information. The upper plot (a) is concerned with the power loss depending on the relation d/a, whereas the lower plot (b) illustrates the explicit dependence of the object size on the target distance.

First, let us discuss subplot (a) of Fig. 6. The black lines show the TCR power-losses and act as upper bounds on the possible power-losses expected from real targets. With the previously obtained maximal power-losses, i.e., -50 dB and -80 dB, we are able to introduce the green area marking the range of feasible scenarios. The blue areas are introduced by allowing one parameter to be loosened, i.e., either the antenna gain or the permissible power loss is increased. The orange area marks scenarios where both mentioned parameters have to be loosened, which we assume to result in improbable measurement scenarios. The maximally feasible distance can be expected at $d \approx 40a$. With some relaxations, we may extend this range to at most $d \approx 200a$.

Let us now discuss subplot (b) of Fig. 6. Here we use the TCR and (43) to obtain lower bounds on the required object size (black lines).

The orange lines act as relative object size limits. For practical reasons, we limit the object size to be one order of magnitude below the distance, or at most in the same order of magnitude.

The red lines are absolute size limits. We do not expect relevant targets with sizes above several 10 m, but definitely not above 100 m.

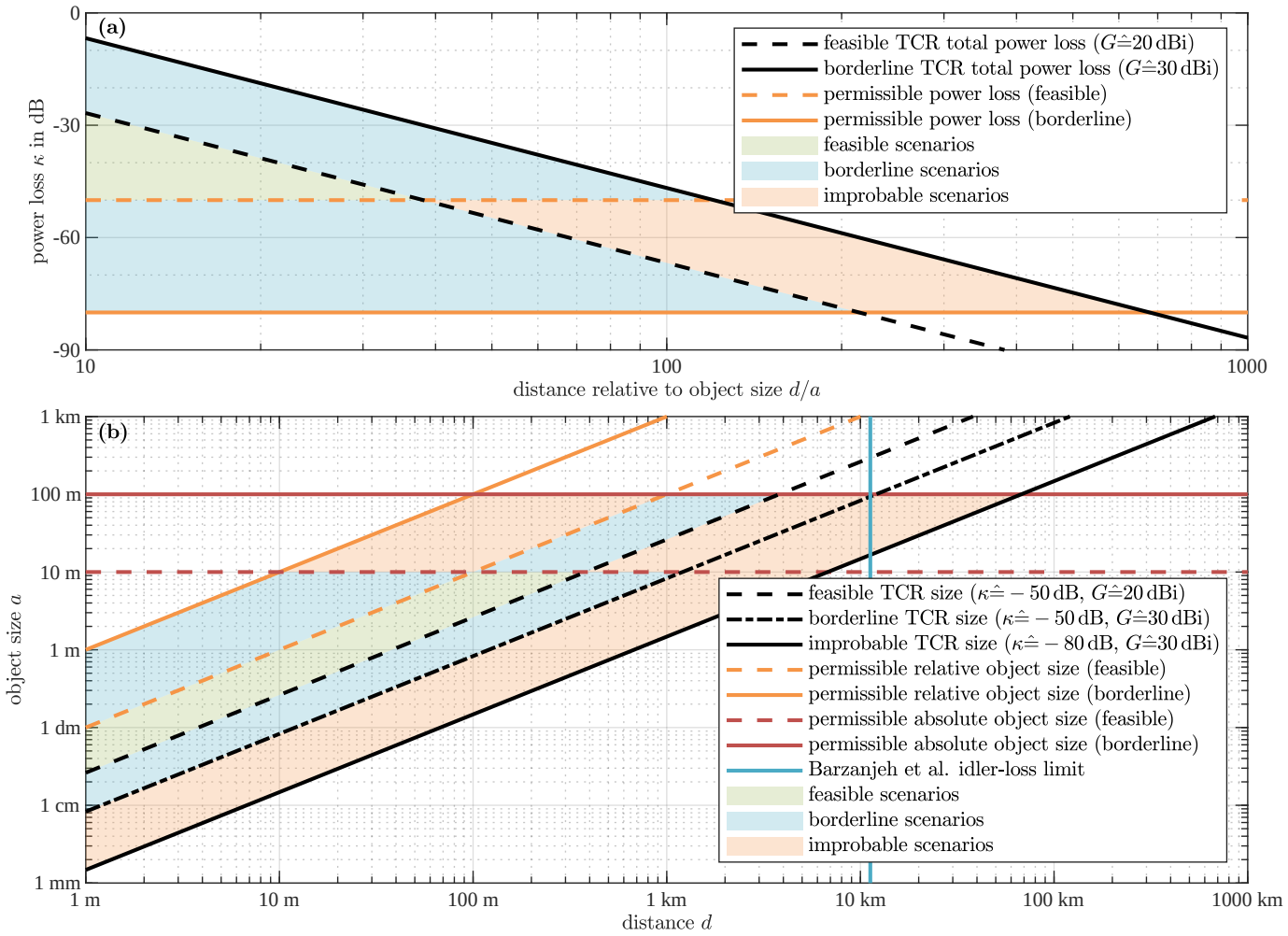

Fig. 6. Overview of possible radar scenarios depending on the target size, object distance and signal power-loss.

In [5], it is concluded that the maximum detection range of the quantum radar is given by the power loss of the idler signal due to the physical length of the storage wave-guide that introduces the necessary time delay with respect to the measurement path. Barzanjeh et al. arrive at an optimistic approximation using the power loss of an optical fiber that acts as an intermediate storage for the microwave signal. Losses of the microwave-to-optical and optical-to-microwave conversion are neglected. They compute a maximum detection range of 11.25 km. This idler-loss limit is drawn as a solid blue line in subplot (b) of Fig. 6.

As for the previous analysis, the green area marks the range of feasible scenarios, the blue area is obtained by relaxing one condition, and the orange area by loosening two or more conditions. In addition to this, we have to require that the total power loss may not exceed -50 dB in the green area.

The maximal feasible target distance can then be found at approximately 300 m. It is important to note that the required target size is already 10 m, which borders already at the maximally permissible size limit. In addition to this, the target has to be of the same size as a TCR and deliver the same reflected signal power. Such a coincidence may be regarded as unlikely.

For cases where it is possible to use higher gain antennas (i.e., $G\hat{=}30$ dBi), it might be possible to extend the measurement range to at most 1 km. Again, the target has to be of the same size as the TCR, i.e., 10 m.

To conclude this analysis, we expect relevant scenarios in the close-range regime with distances of several 10 m and object dimensions in the order of 1 m. These distances are well below the idler-loss limit of 11.25 km [5].

VI. Conclusion

In this article, we have provided an overview on the state-of-the-art of quantum radar technology, which is currently considered to be experimentally implementable. In addition to this, we have shown an overview on the classical comparison radar that is described using quantum-mechanical formulations as well as their conventional counterparts. The four presented system setups where analyzed by computing the respective ROCs. We where able to show that the classic signal theoretic approaches of computing the ROCs are the high-power limits of the quantum-mechanical derivations.

Based on the derived ROCs, we have analyzed the applicability of the current quantum radar technology. Our analysis can be applied to future developments as well, as it is possible

to generalize the methodology as we have shown by analyzing the experiment of Assouly et al. [1].

Our analysis shows that the quantum advantage is not only limited to extreme power regimes (i.e., low SNR and high noise power), but that it scales over-proportionally by reducing the available SNR. We also found that there exists for any given quantum advantage a noise power threshold, below which this quantum advantage is not realizable.

Furthermore, we quantified the measurement expense by means of the necessary total measurement time in order to achieve appropriate ROC curves (parametrized and limited by $P_{\mathrm{E,min}} < 25\,\%$, see (21)). We come to the conclusion that, for practical applications, the total power-loss has to be better then -50 dB. With such a power loss, the measurement duration can be expected to be in the order of milliseconds. We expect that feasible measurement scenarios, in which a quantum radar outperforms a classic radar, may only be found in the near-range (distances less then approximately 300 m).

It is possible to argue that future developments, such as a parallel operation of quantum radars at different signal frequencies, may decrease the measurement time and allow to extend viable detection scenarios to increased power losses. However, this parallelization can also be implemented for the classic radar and the quantum advantage would again be limited to the single-frequency case. The question that arises is whether a 2 dB, 3 dB or even a 6 dB SNR (or sample number) advantage is necessary, when the price for this is to decrease the transmitted signal power levels to -10 dB (2 dB quantum advantage) or even to -55 dB (3 dB quantum advantage) below the thermal noise power.

It is important to mention that the existing quantum radar and quantum illumination concepts are constantly being developed further, and effects different or beyond entanglement are being added to the list of exploitable phenomena. With the so-called *hyperentanglement*, Prabhu et al. expect a quantum advantage of 12 dB [62]. Fancher et al. show in their review article [63] how *Rydberg atom electric field sensors* may be used to benefit conventional radio frequency receivers. This would, as stated by Fancher et al., allow for "[...] small-size, highly sensitive, and broadly tunable [sensors with, F.B.] the potential for performing precision vector electric field and angle-of-arrival measurements." Independent of further technological advancements or newly tamed effects, the principles and the approach presented in our article can be applied to those and other proposals as well, provided that statistical moments and ROC curves are obtainable.

In order for the quantum radar technology to be able to compete with the established field of conventional radar technology, it seems necessary to translate the existing capabilities and advantages of generating and using entangled pairs of microwave photons to the high-power and -SNR regime.

A further application for low-power quantum radar may be found in medicine [64] or cell biology. A demonstration on the electromagnetic characterization of cells is given in [65], [66], where the authors probe individual cells. There, the electric field-strength is of crucial importance, as strong fields may cause the cell to deform and change its behavior [65]. This is where quantum-radar technology might be of assistance.

APPENDIX

This appendix contains the derivation of the statistical moments shown in Table I, which are used in the ROC curves and the detection performance analysis herein. We first provide an overview of the two classic setups and discuss then the two quantum formulations.

A. Classic Signal Theory

The following section contains an overview of the principle conventional radar setups with a strictly classical signal theoretic modeling.

For the treatment of both conventional setups, we introduce the measurement noise as a time dependent random variable $\mathsf{Z}(t)$, with time t, and the baseband quadrature amplitudes as the time dependent random variables $\mathsf{Z}_{\mathrm{X}}(t)$ and $\mathsf{Z}_{\mathrm{P}}(t)$. We get

$$\mathsf{Z}(t) = \mathsf{Z}_{\mathrm{X}}(t)\cos(2\pi f t) + \mathsf{Z}_{\mathrm{P}}(t)\sin(2\pi f t), \tag{50}$$

with the carrier frequency f.

1) The unmodulated continuous-wave radar: The U-CW transmit signal is defined by the quadrature amplitude x_{T} and is given as

$$s_{\mathrm{T}}(t) = x_{\mathrm{T}}\cos(2\pi f t). \tag{51}$$

The receive signal, due to the added measurement noise, is given as the time dependent random variable $\mathsf{S}_{\mathrm{R}}(t)$ yielding

$$\begin{aligned}\mathsf{S}_{\mathrm{R}}(t) = \left(\sqrt{\kappa}x_{\mathrm{T}} + \mathsf{Z}_{\mathrm{X}}(t)\right)\cos(2\pi f t) + \\ \mathsf{Z}_{\mathrm{P}}(t)\sin(2\pi f t)\,.\end{aligned} \tag{52}$$

The quadrature detector and the data acquisition (see subplot (b) in Fig. 1) perform a transformation of the received signal $\mathsf{S}_{\mathrm{R}}(t)$ that results in a discrete-time series of observations of the quadrature that contains the signal portion $\sqrt{\kappa}x_{\mathrm{T}}$. The noise contained in the other quadrature is rejected through this process. Successive snapshots of independent samples of the measured quantity are enumerated by m. The samples of the measured quadrature amplitudes are denoted as X_m and are given as

$$\mathsf{X}_m = \sqrt{\kappa}x_{\mathrm{T}} + \mathsf{Z}_m^{\mathrm{X}}. \tag{53}$$

Herein, the random variable $\mathsf{Z}_m^{\mathrm{X}}$ is the baseband measurement noise $\mathsf{Z}_{\mathrm{X}}(\bullet)$ sampled at time instance $T_{\mathrm{S}}m$ yielding

$$\mathsf{Z}_m^{\mathrm{X}} = \mathsf{Z}_{\mathrm{X}}(T_{\mathrm{S}}m), \tag{54}$$

where T_{S} is the sample interval.

We assume that the measurement noise follows a Gaussian distribution and that the sample interval is such, that the $\mathsf{Z}_m^{\mathrm{X}}$ are independent and identically distributed (iid). It follows that

$$\mathsf{Z}_m^{\mathrm{X}} \sim \mathcal{N}\left(0;\sigma_{\mathsf{Z}}^2\right), \tag{55}$$

$$\text{and}\quad \mathsf{X}_m \sim \mathcal{N}\left(\sqrt{\kappa}x_{\mathrm{T}};\sigma_{\mathsf{Z}}^2\right). \tag{56}$$

The signal-to-noise ratio (SNR) is computed as the ratio of the received signal power without noise (i.e., $\sigma_{\mathsf{Z}}^2 = 0$) to the received signal power without a transmit signal present

(i.e., $x_\mathrm{T} = 0$). For the first case, the received signal is purely deterministic so that the average power can be computed as

$$\lim_{T\to\infty} T^{-1} \int_{-T/2}^{T/2} \mathrm{E}\big[\, \mathsf{S}_\mathrm{R}^2(t) \big|\, \sigma_\mathsf{Z}^2 = 0\big] \mathrm{d}t = \frac{\kappa x_\mathrm{T}^2}{2}. \tag{57}$$

Herein, the averaging time T is introduced for the purpose of integration. For the latter case, the received signal is purely stochastic so that the mean power yields

$$\mathrm{E}\big[\mathsf{S}_\mathrm{R}^2(t) | x_\mathrm{T} = 0\big] = \sigma_\mathsf{Z}^2. \tag{58}$$

With (57) and (58) we formulate the SNR r as

$$r = \frac{\kappa x_\mathrm{T}^2}{2\sigma_\mathsf{Z}^2}. \tag{59}$$

2) The ideal noise-radar: The noise radar's generator signal comprises the time-dependent random baseband quadrature variables $\mathsf{X}(t)$ and $\mathsf{P}(t)$. The transmitted, idler and received signal are thus given as

$$\begin{aligned} \mathsf{S}_\mathrm{T}(t) &= \mathsf{S}_\mathrm{I}(t) && (60)\\ &= \mathsf{X}(t)\cos(2\pi f t) + \mathsf{P}(t)\sin(2\pi f t)\,, && (61)\\ \text{and}\quad \mathsf{S}_\mathrm{R}(t) &= \big(\sqrt{\kappa}\mathsf{X}(t) + \mathsf{Z}_\mathrm{X}(t)\big)\cos(2\pi f t) + \\ &\quad \big(\sqrt{\kappa}\mathsf{P}(t) + \mathsf{Z}_\mathrm{P}(t)\big)\sin(2\pi f t)\,. && (62) \end{aligned}$$

We introduce the random quadrature variables X_m and P_m of the transmitted signal as samples taken at time instances $T_\mathrm{S} m$ as

$$\mathsf{X}_m = \mathsf{X}(T_\mathrm{S} m) \quad \text{and} \quad \mathsf{P}_m = \mathsf{P}(T_\mathrm{S} m). \tag{63}$$

The radar receiver performs a correlation of the measurement and idler quadrature amplitudes. The correlator output is denoted by the random variable C_m and defined as

$$\begin{aligned} \mathsf{C}_m = &\big(\sqrt{\kappa}\mathsf{X}_m + \mathsf{Z}_m^\mathrm{X}\big)\mathsf{X}_m + \\ &\big(\sqrt{\kappa}\mathsf{P}_m + \mathsf{Z}_m^\mathrm{P}\big)\mathsf{P}_m, \end{aligned} \tag{64}$$

where we have introduced the sample Z_m^P analog to Z_m^X given in (54).

By assuming that samples of the transmit signal's quadrature amplitudes are Gaussian distributed and iid with variance σ_S^2, we get

$$\mathsf{X}_m, \mathsf{P}_m \sim \mathcal{N}\big(0, \sigma_\mathsf{S}^2\big). \tag{65}$$

Consequently, the first and second order central moments of the correlation variable C_m are

$$\begin{aligned} \mathrm{E}[\mathsf{C}_m] &= 2\sqrt{\kappa}\sigma_\mathsf{S}^2, && (66)\\ \text{and}\quad \mathrm{Var}[\mathsf{C}_m] &= 4\kappa\sigma_\mathsf{S}^4 + 2\sigma_\mathsf{S}^2\sigma_\mathsf{Z}^2. && (67) \end{aligned}$$

The SNR is computed as the ratio of the receive signal's variance $\mathsf{S}_\mathrm{R}(t)$ without noise (i.e., $\sigma_\mathsf{Z}^2 = 0$) to the receive-signal's variance without a transmit signal being present (i.e., $\sigma_\mathsf{S}^2 = 0$). The SNR is given as

$$r = \frac{\mathrm{E}\big[\mathsf{S}_\mathrm{R}^2(t) | \sigma_\mathsf{Z}^2 = 0\big]}{\mathrm{E}\big[\mathsf{S}_\mathrm{R}^2(t) | \sigma_\mathsf{S}^2 = 0\big]} = \frac{\kappa\sigma_\mathsf{S}^2}{\sigma_\mathsf{Z}^2}. \tag{68}$$

B. Quantum-Mechanical Formulations

The previous derivations established that the relevant quantities in the analysis of the radar schemes are the quadrature amplitudes. In the following quantum-mechanical treatment, the random variables used in modeling the noisy quadrature signals are replaced by quantum mechanical operators that describe the quantized electromagnetic field. Thus, the quantized quadratures are represented by the operators $\hat{x}$ and $\hat{p}$. In addition, it is common to introduce the operator $\hat{a}$ as

$$\hat{a} = \hat{x} + \mathrm{i}\hat{p}, \tag{69}$$

with i being the imaginary unit. Consequently, it is possible to express the quadrature operators as

$$\hat{x} = \frac{1}{2}\big(\hat{a} + \hat{a}^\dagger\big) \tag{70}$$

$$\text{and}\quad \hat{p} = \frac{1}{2\mathrm{i}}\big(\hat{a} - \hat{a}^\dagger\big), \tag{71}$$

with $\hat{a}^\dagger$ being the adjoint operator to $\hat{a}$. Note that $\hat{a}$ and $\hat{a}^\dagger$ are also known as the bosonic annihilation and creation operators, respectively [67].

By analogy, it is possible to regard the operator $\hat{a}$ as the complex amplitude of a signal or random sequence. Similarly, it can be used to compute the power of the associated signal. To this end, a "power operator" $\hat{n}$ is introduced as

$$\hat{n} = \hat{a}^\dagger\hat{a}, \tag{72}$$

which is referred to as number operator. The expected (photon) number N is given as

$$N = \langle\psi|\hat{n}|\psi\rangle = \langle\hat{n}\rangle\,. \tag{73}$$

Herein, $|\psi\rangle$ is a state vector that is used for the task of computing a statistical moment in a similar capacity as a probability density function in classic signal theory.

The mean photon number N can be treated as the signal power. However, it is normalized to the energy content carried by a single photon and the timespan of a detection window. From [2] it follows for the relation between the signal power P and the photon number that

$$N \approx \frac{P}{hfW}. \tag{74}$$

Herein, h is Planck's constant, f is the signal's frequency and W is the phase matching bandwidth, which is analogous to the bandwidth of the signal. The photon number is therefore proportional to the signal's power and can be used interchangeably.

In the following, we indicate the signal or system specific operators by the superscripts T for transmit, R for receive, I for idler, S for signal and B for the added background-noise in the measurement path.

Additive measurement noise is modeled as a thermal state which is subject to the bosonic annihilation-operator $\hat{a}_m^\mathrm{B}$, where m is used to enumerate successive experiments. The corresponding expectation value of the photon number operator is obtained as

$$(1-\kappa)\left\langle \big(\hat{a}_m^\mathrm{B}\big)^\dagger \hat{a}_m^\mathrm{B} \right\rangle = N_\mathrm{th}. \tag{75}$$

Herein, N_{th} is the mean noise-photon number that is injected into the radar's receive unit. The scaling by $1-\kappa$ is due to the noise injection using a signal coupler with the power-coupling factor κ [2]. The effective noise-photon number observable at the receiver is then, as we will see later on, independent of κ.

The noise-photon number is computed using the Bose-Einstein distribution depending on the temperature T and the frequency f as [2]

$$N_{\text{th}} = \left(\exp\left\{ \frac{h/k_{\text{B}}}{T/f} \right\} - 1 \right)^{-1}. \tag{76}$$

Herein, k_{B} is Boltzmann's constant.

1) The coherent-state formulation: The state vector $|\psi_{\text{COH}}\rangle$ of the coherent state signal is given by [2] as

$$|\psi_{\text{COH}}\rangle = \exp\left\{ -\frac{1}{2}|\lambda|^2 \right\} \sum_{n=0}^{\infty} \frac{\lambda^n}{\sqrt{n}} |n\rangle, \tag{77}$$

with $\lambda \in \mathbb{C}$ defining the signal power, i.e., the photon number and the mean value of the quadrature amplitudes. In the following, we assume without loss of generality $\lambda = |\lambda|$. The $|n\rangle$ are Fock basis-vectors.

The quadrature amplitudes of the transmitted signal are $\hat{x}_m^{\text{T}}$ and $\hat{p}_m^{\text{T}}$. Their respective expectation values are

$$\left\langle \hat{x}_m^{\text{T}} \right\rangle = \lambda \tag{78}$$

$$\text{and} \quad \left\langle \hat{p}_m^{\text{T}} \right\rangle = 0. \tag{79}$$

The mean signal photon number N_{S} of the transmitted signal is obtained as

$$N_{\text{S}} = \left\langle \left(\hat{a}_m^{\text{T}}\right)^\dagger \hat{a}_m^{\text{T}} \right\rangle \tag{80}$$

$$= |\lambda|^2. \tag{81}$$

After the interaction of the probe signal with the measurement environment and the injection of noise, we arrive at the annihilation operator $\hat{a}_m^{\text{R}}$, applicable to describe the signal at the receiver input, as

$$\hat{a}_m^{\text{R}} = \sqrt{\kappa}\hat{a}_m^{\text{T}} + \sqrt{1-\kappa}\hat{a}_m^{\text{B}}. \tag{82}$$

Thus, the received mean photon number N_{R} is

$$N_{\text{R}} = \left\langle \left(\hat{a}_m^{\text{R}}\right)^\dagger \hat{a}_m^{\text{R}} \right\rangle \tag{83}$$

$$= \kappa N_{\text{S}} + N_{\text{th}}. \tag{84}$$

We define the SNR as the ratio of the received mean photon number for the case where there is on-average no noise (i.e., $N_{\text{th}} = 0$) to the case where there is on-average no signal (i.e., $N_{\text{S}} = 0$). The SNR r yields

$$r = \frac{N_{\text{R}}|_{N_{\text{th}}=0}}{N_{\text{R}}|_{N_{\text{S}}=0}} \tag{85}$$

$$= \frac{\kappa N_{\text{S}}}{N_{\text{th}}}. \tag{86}$$

The discussed receiver performs a measurement of the quadrature amplitude in-phase with the transmitted signal. The associated measurement operator is $\hat{x}_m$ and defined as

$$\hat{x}_m = \frac{1}{2}\left(\hat{a}_m^{\text{R}} + \left(\hat{a}_m^{\text{R}}\right)^\dagger \right). \tag{87}$$

The first- and second-order central-moments are thus calculated as

$$\langle \hat{x}_m \rangle = \sqrt{\kappa}\lambda, \tag{88}$$

$$\text{and} \quad \left\langle \left(\hat{x}_m - \langle \hat{x}_m \rangle\right)^2 \right\rangle = \frac{1}{4}(2N_{\text{th}} + 1), \tag{89}$$

respectively. The computational steps leading to (88) and (89) are not shown in here. However, a similar derivation can be found in the supplement material of [9].

2) The two-mode squeezed vacuum quantum-radar: The quantum radar's transmit state-vector $|\psi_{\text{TMSV}}\rangle$ is given as

$$|\psi_{\text{TMSV}}\rangle = \sum_{n=0}^{\infty} \sqrt{\frac{N_{\text{S}}^n}{(1+N_{\text{S}})^{n+1}}} |n\rangle_{\text{S}} |n\rangle_{\text{I}}. \tag{90}$$

Herein, the Fock basis-vectors $|n\rangle_{\text{S}}$ and $|n\rangle_{\text{I}}$ refer to the modes routed via the signal path and the idler path, respectively [2], [67], [68]. The mean photon number of both, the transmitted measurement- and the retained idler-signals, are

$$N_{\text{S}} = \left\langle \left(\hat{a}_m^{\text{T}}\right)^\dagger \hat{a}_m^{\text{T}} \right\rangle \tag{91}$$

$$= \left\langle \left(\hat{a}_m^{\text{I}}\right)^\dagger \hat{a}_m^{\text{I}} \right\rangle. \tag{92}$$

The measurement path of the TMSV setup acts on the transmitted signal in the same way, as it is the case for the coherent state approach. The annihilation operator of the received signal is therefore given by (82) as well, and the mean photon number of the received signal is given by (84). The SNR is in this case again given by (86).

The measurement operator to be realized within the TMSV setup describes a correlation with respect to the quadrature amplitudes of the measurement and the idler signal-paths [9]. With $\hat{x}_m^{\text{R}}$ and $\hat{p}_m^{\text{R}}$ being the quadrature operators of the received signal, and $\hat{x}_m^{\text{I}}$ and $\hat{p}_m^{\text{I}}$ being the quadrature operators of the idler signal, the correlation operator follows as

$$\hat{c}_m = \hat{x}_m^{\text{R}}\hat{x}_m^{\text{I}} - \hat{p}_m^{\text{R}}\hat{p}_m^{\text{I}}. \tag{93}$$

The first order moment of $\hat{c}_m$ is

$$\langle \hat{c}_m \rangle = \sqrt{\kappa N_{\text{S}}(1+N_{\text{S}})}, \tag{94}$$

and the second order central moment yields

$$\begin{aligned} \left\langle \left(\hat{c}_m - \langle \hat{c}_m \rangle\right)^2 \right\rangle = & \frac{1}{4} + \kappa\left(N_{\text{S}} + N_{\text{S}}^2\right) + \\ & \frac{1}{4}(2N_{\text{th}}N_{\text{S}} + N_{\text{th}} + (1-\kappa)N_{\text{S}}). \end{aligned} \tag{95}$$

Again, the computational steps leading to (94) and (95) are not shown in here. However, a similar derivation can be found in the supplement material of [9].

REFERENCES

[1] R. Assouly, R. Dassonneville, T. Peronnin, A. Bienfait, and B. Huard, "Quantum advantage in microwave quantum radar," *Nat. Phys.*, pp. 1–5, 2023.

[2] G. Sorelli, N. Treps, F. Grosshans, and F. Boust, "Detecting a target with quantum entanglement," *IEEE Aerosp. Electron. Syst. Mag.*, vol. 37, no. 5, pp. 68–90, 2022.

[3] D. Luong, B. Balaji, C. W. Sandbo Chang, V. M. Ananthapadmanabha Rao, and C. Wilson, "Microwave quantum radar: An experimental validation," in *2018 International Carnahan Conference on Security Technology (ICCST)*. IEEE, 2018, pp. 1–5.

[4] D. Luong, C. W. S. Chang, A. M. Vadiraj, A. Damini, C. M. Wilson, and B. Balaji, "Receiver operating characteristics for a prototype quantum two-mode squeezing radar," *IEEE Trans. Aerosp. Electron. Syst.*, vol. 56, no. 3, pp. 2041–2060, 2020.

[5] D. S. Barzanjeh, D. S. Pirandola, D. Vitali, and M. J. Fink, "Microwave quantum illumination with a digital phase-conjugated receiver," *IEEE Radar Conference*, p. 6, 2020.

[6] R. Di Candia, H. Yiğitler, G. Paraoanu, and R. Jäntti, "Two-way covert quantum communication in the microwave regime," *PRX Quantum*, vol. 2, no. 2, 2021.

[7] S. Guha and B. I. Erkmen, "Gaussian-state quantum-illumination receivers for target detection," *Phys. Rev. A*, vol. 80, no. 5, p. 052310, 2009.

[8] S. Barzanjeh, S. Guha, C. Weedbrook, D. Vitali, J. H. Shapiro, and S. Pirandola, "Microwave quantum illumination," *Phys. Rev. Lett.*, vol. 114, no. 8, p. 080503, 2015.

[9] U. Las Heras, R. Di Candia, K. G. Fedorov, F. Deppe, M. Sanz, and E. Solano, "Quantum illumination reveals phase-shift inducing cloaking," *Sci Rep*, vol. 7, no. 1, p. 9333, 2017.

[10] H. Shi, B. Zhang, and Q. Zhuang, "Fulfilling entanglement's optimal advantage via converting correlation to coherence," *arXiv:2207.06609*, 2023.

[11] ——, "Fulfilling entanglement's optimal advantage via converting correlation to coherence," in *CLEO 2023*. Optica Publishing Group, 2023.

[12] J. Angeletti, H. Shi, T. Lakshmanan, D. Vitali, and Q. Zhuang, "Microwave quantum illumination with correlation-to-displacement conversion," *Phys. Rev. Applied*, vol. 20, no. 2, p. 024030, 2023.

[13] M. Reichert, Q. Zhuang, J. H. Shapiro, and R. Di Candia, "Quantum illumination with a hetero-homodyne receiver and sequential detection," *Phys. Rev. Applied*, vol. 20, no. 1, p. 014030, 2023.

[14] Z. Huang, C. Lupo, and P. Kok, "Quantum-limited estimation of range and velocity," *PRX Quantum*, vol. 2, no. 3, p. 030303, 2021.

[15] M. Reichert, R. Di Candia, M. Z. Win, and M. Sanz, "Quantum-enhanced doppler lidar," *npj Quantum Inf*, vol. 8, 2022.

[16] R. Jäntti, R. Di Candia, R. Duan, and K. Ruttik, "Multiantenna quantum backscatter communications," in *2017 IEEE Globecom Workshops (GC Wkshps)*, 2017, pp. 1–6.

[17] D. Luong, S. Rajan, and B. Balaji, "Are quantum radar arrays possible?" in *2019 IEEE International Symposium on Phased Array System & Technology (PAST)*, 2019, pp. 1–4.

[18] D. M. Frasca and D. A. Farina, "Multiple input-multiple output quantum radar," *IEEE Radar Conference*, p. 4, 2020.

[19] R. Loudon, *The Quantum Theory of Light*. OUP Oxford, 2000.

[20] S. Lloyd, "Enhanced sensitivity of photodetection via quantum illumination," *Science*, vol. 321, no. 5895, pp. 1463–1465, 2008.

[21] S.-H. Tan, B. I. Erkmen, V. Giovannetti, S. Guha, S. Lloyd, L. Maccone, S. Pirandola, and J. H. Shapiro, "Quantum illumination with gaussian states," *Phys. Rev. Lett.*, vol. 101, no. 25, 2008.

[22] D. Luong, *Quantum Radar Signal Processing*. Carleton University, 2023.

[23] G. De Palma and J. Borregaard, "The minimum error probability of quantum illumination," *Phys. Rev. A*, vol. 98, no. 1, 2018.

[24] R. Nair and M. Gu, "Fundamental limits of quantum illumination," *Optica*, vol. 7, no. 7, 2020.

[25] M. Bradshaw, L. O. Conlon, S. Tserkis, M. Gu, P. K. Lam, and S. M. Assad, "Optimal probes for continuous-variable quantum illumination," *Phys. Rev. A*, vol. 103, no. 6, 2021.

[26] J. H. Shapiro, "The quantum illumination story," *IEEE Aerospace and Electronic Systems Magazine*, vol. 35, no. 4, pp. 8–20, 2020.

[27] R. Jonsson and R. Di Candia, "Gaussian quantum estimation of the loss parameter in a thermal environment," *J. Phys. A: Math. Theor.*, vol. 55, no. 38, 2022.

[28] Z. Gong, N. Rodriguez, C. N. Gagatsos, S. Guha, and B. A. Bash, "Quantum-enhanced transmittance sensing," *IEEE Journal of Selected Topics in Signal Processing*, vol. 17, no. 2, 2023.

[29] U. Lübbert, *Target Position Estimation with a Continuous Wave Radar Network*. Cuvillier Verlag, 2005.

[30] A. Gyasi-agyei, *Wireless Internet Of Things: Principles And Practice*. World Scientific, 2020.

[31] Q. Zhuang, Z. Zhang, and J. H. Shapiro, "Optimum mixed-state discrimination for noisy entanglement-enhanced sensing," *Phys. Rev. Lett.*, vol. 118, no. 4, 2017.

[32] X. Chen and Q. Zhuang, "Entanglement-assisted detection of fading targets via correlation-to-displacement conversion," *Phys. Rev. A*, vol. 107, no. 6, p. 062405, 2023-06-05.

[33] D. Luong, B. Balaji, and S. Rajan, "Quantum radar: Challenges and outlook: An overview of the state of the art," *IEEE Microwave Magazine*, vol. 24, no. 9, pp. 61–67, 2023.

[34] C. W. S. Chang, A. M. Vadiraj, J. Bourassa, B. Balaji, and C. M. Wilson, "Quantum-enhanced noise radar," *Applied Physics Letters*, vol. 114, no. 11, p. 112601, 2019.

[35] K. Kulpa, *Signal Processing in Noise Waveform Radar*. Artech House, 2013.

[36] R. Jonsson and M. Ankel, "Quantum radar – what is it good for?" in *2021 IEEE Radar Conference (RadarConf21)*, 2021, pp. 1–6.

[37] D. Luong, S. Rajan, and B. Balaji, "Quantum two-mode squeezing radar and noise radar: Correlation coefficients for target detection," *IEEE Sensors Journal*, vol. 20, no. 10, pp. 5221–5228, 2020.

[38] D. Luong, B. Balaji, and S. Rajan, "Quantum two-mode squeezing radar and noise radar: Correlation coefficient and integration time," *IEEE Access*, vol. 8, pp. 185 544–185 547, 2020.

[39] ——, "Performance prediction for coherent noise radars using the correlation coefficient," *IEEE Access*, vol. 10, pp. 8627–8633, 2022.

[40] ——, "Structured covariance matrix estimation for noise-type radars," *IEEE Transactions on Geoscience and Remote Sensing*, vol. 60, pp. 1–13, 2022.

[41] ——, "Noise-type radars: Probability of detection vs. correlation coefficient and integration time," *arXiv:2208.03417*, 2022.

[42] J. A. Russer, M. Würth, W. Utschick, F. Bischeltsrieder, and M. Peichl, "Performance considerations for quantum radar," in *2021 International Applied Computational Electromagnetics Society Symposium (ACES)*, 2021, pp. 1–4.

[43] R. Wei, J. Li, W. Wang, and Q. Guo, "Investigation on the advantages of quantum illumination radar by using radar equation," in *2021 CIE International Conference on Radar (Radar)*, 2021, pp. 2816–2820.

[44] R. Wei, J. Li, W. Wang, Z. Ye, C. Zhao, and Q. Guo, "Evaluating the detection range of microwave quantum illumination radar," *IET Radar, Sonar & Navigation*, 2023.

[45] R. Gallego Torromé and S. Barzanjeh, "Advances in quantum radar and quantum LiDAR," *Progress in Quantum Electronics*, p. 100497, 2023.

[46] A. Karsa, A. Fletcher, G. Spedalieri, and S. Pirandola, "Quantum illumination and quantum radar: A brief overview," *arXiv:2310.06049*, 2023.

[47] M. Dawood and R. Narayanan, "Receiver operating characteristics for the coherent UWB random noise radar," *IEEE Trans. Aerosp. Electron. Syst.*, vol. 37, no. 2, pp. 586–594, 2001.

[48] R. M. Dudley, *Uniform Central Limit Theorems*. Cambridge University Press, 1999.

[49] S. M. Kay, *Detection theory*, 14th ed., ser. Fundamentals of Statistical Signal Processing. Prentice Hall PTR, 2009, no. 2.

[50] R. Jonsson, R. Di Candia, M. Ankel, A. Ström, and G. Johansson, "A comparison between quantum and classical noise radar sources," in *2020 IEEE Radar Conference (RadarConf20)*, 2020, pp. 1–6.

[51] K. Yao, F. Lorenzelli, and C.-E. Chen, *Detection and Estimation for Communication and Radar Systems*. Cambridge University Press, 2013.

[52] F. Nielsen, "Chernoff information of exponential families," *arXiv:1102.2684 [cs.IT]*, 2011.

[53] D. Luong, B. Balaji, and S. Rajan, "Speeding up detection and imaging using quantum radars," in *2023 IEEE International Conference on Acoustics, Speech, and Signal Processing Workshops (ICASSPW)*, 2023, pp. 1–5.

[54] D. K. Barton, *Radar System Analysis and Modeling*. Artech House, 2004.

[55] T. A. Milligan, *Modern Antenna Design*. John Wiley & Sons, 2005.

[56] *Zynq™ UltraScale+™ RFSoC Product Brief*. Xilinx, December 20, 2023.

[57] *R&S® RTP High-Performance Oscilloscope Data Sheet*. Rohde & Schwarz, December 20, 2023.

[58] M. K. A. Thumm, W. Wiesbeck, and S. Kern, *Hochfrequenzmeßtechnik: Verfahren und Meßsysteme*, 2nd ed. Vieweg + Teubner, 2008.

[59] D. Arweiler, *Multi-SQUID Josephson Parametric Amplifiers*. Technische Universität München (TUM), 2018.

[60] F. T. Ulaby, R. K. Moore, and A. K. Fung, *Microwave remote sensing. 2: Radar remote sensing and surface scattering and emission theory*, ser. Remote sensing. Addison-Wesley, 1982, no. 3.

[61] W. Stutzman, "Estimating directivity and gain of antennas," *IEEE Antennas Propag. Mag.*, vol. 40, no. 4, pp. 7–11, 1998.

[62] A. V. Prabhu, B. Suri, and C. M. Chandrashekar, "Hyperentanglement-enhanced quantum illumination," *Phys. Rev. A*, vol. 103, no. 5, 2021.

[63] C. T. Fancher, D. R. Scherer, M. C. S. John, and B. L. S. Marlow, "Rydberg atom electric field sensors for communications and sensing," *IEEE Transactions on Quantum Engineering*, vol. 2, pp. 1–13, 2021.

[64] D. Luong, B. Balaji, and S. Rajan, "Biomedical sensing using quantum radars based on josephson parametric amplifiers," *2021 International Applied Computational Electromagnetics Society Symposium (ACES)*, pp. 1–4, 2021.
[65] J. C. Hwang, "Label-free noninvasive cell characterization: A methodology using broadband impedance spectroscopy," *IEEE Microwave Magazine*, vol. 22, no. 5, pp. 78–87, 2021.
[66] X. Du, C. Ladegard, X. Ma, X. Cheng, and J. C. Hwang, "Broadband electrical sensing of nucleus size in a live cell from 900 hz to 40 GHz," *2020 IEEE MTT-S International Microwave Biomedical Conference (IMBioC)*, pp. 1–4, 2020.
[67] S. L. Braunstein and P. van Loock, "Quantum information with continuous variables," *Rev. Mod. Phys.*, vol. 77, no. 2, pp. 513–577, 2005.
[68] C. Weedbrook, S. Pirandola, R. García-Patrón, N. J. Cerf, T. C. Ralph, J. H. Shapiro, and S. Lloyd, "Gaussian quantum information," *Rev. Mod. Phys.*, vol. 84, pp. 621–669, May 2012.

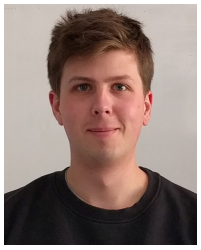

Florian Bischeltsrieder received the B.Sc. degree in engineering physics from the Munich University of Applied Sciences (HM), Germany, in 2015 and the M.Sc. degree in electrical engineering and information technology from the Technical University of Munich (TUM), Germany, in 2017, both with high distinction. In 2018, he joined the Microwaves and Radar Institute of the German Aerospace Center (DLR) where he is currently a research associate and pursuing a doctoral degree under the supervision of Wolfgang Utschick (TUM). His current research interests include radar imaging, signal processing and quantum radar.

Michael Würth received the B.Sc. and M.Sc. (with high distinction) degrees in electrical engineering and information technology from Technische Universität München (TUM), Germany, in 2017 and 2020, respectively. In 2019, he joined the Professorship of Signal Processing Methods (MSV) at TUM, where he is currently a research assistant and a doctoral candidate. His current research interests include signal processing and its application to quantum radar.

Johannes Russer (S'02–GSM'05–M'09) received the M.S.E.E. degree in electrical engineering and information technology from the Karlsruhe Institute of Technology, Karlsruhe, Germany, in 2003, the Ph.D.E.E. degree from the University of Illinois at Urbana-Champaign, Champaign, IL, USA, in 2010, and the Dr.-Ing. habil. degree from the Technical University of Munich (TUM), Munich, Germany, in 2017. In 2018, he joined eV-Technologies, Caen, France.

In 2004, he joined the University of Illinois at Urbana-Champaign as a Research Assistant. From 2007 to 2010, he was an Intern with Qualcomm Inc. Since 2010, he been a Postdoctoral Research Fellow with the Institute of Nanoelectronics, TUM, where he is involved in multiphysics modeling in nanoelectronics, quantum circuit theory, wireless power transfer, and in the area of stochastic electromagnetic fields. He has authored or coauthored more than 170 scientific papers in refereed journals and conference proceedings.

Dr. Russer is a Member of VDE and the Eta Kappa Nu Honor Society. He received the Best Student Paper Award at the IEEE International Microwave Symposium in 2008 and 2015, and the Best Paper Award from the ITG.

Markus Peichl (Member, IEEE) is holding a Diploma and a PhD in Electrical Engineering, both from Technical University of Karlsruhe (now KIT – Karlsruhe Institute of Technology). He has 32 years of experience in microwave remote sensing. Joining DLR in 1990, he is leading the Microwaves Sensors Group within the Department of Reconnaissance and Security at DLR Microwaves and Radar Institute since 1998. His present interests focus on technology for space-borne, airborne, ground-based and UAV-carried microwave remote sensing systems, especially synthetic aperture radar and microwave radiometers, for a multitude of applications.

Wolfgang Utschick (Fellow, IEEE) received the diploma and doctoral degrees in electrical engineering with distinction from the Technical University of Munich (TUM), Germany, in 1993 and 1998, respectively. Prior to that, he completed several years of certified industrial training programs. Since 2002, he is Professor (Ordinarius) for Methods of Signal Processing and since 2011, he is a TUM Asia faculty member in Singapore and a regular guest Professor with Singapore Institute of Technology. In 2021, he became a core member of the newly founded Munich Data Science Institute. From 2017 to 2022, he served two terms of office as the dean of the Department of Electrical and Computer Engineering at TUM. He is a member of the VDE, where he is deputy head of the specialist group KT 1 for Information and System Theory of the German Information Technology Society (ITG). He also served as an Associate Editor for the IEEE Transactions on Circuits and Systems and for the IEEE Transactions on Signal Processing and was a Member of the IEEE Signal Processing Society Technical Committee on Signal Processing for Communications and Networking. From 2016 till 2022 he was chairing the German Chapter of the IEEE Signal Processing Society, and since 2016, he has been director of the special research group Mobility & Transport of the Bavarian Science Forum BayWISS.

Wolfgang Utschick teaches courses on signal processing, stochastic processes, optimization theory, and machine learning in the field of wireless communications and various other application areas of signal processing, he holds several patents in the field of multiantenna signal processing and has authored and coauthored a large number of technical articles in international journals and conference proceedings. He has edited several books and is the founder and the editor of the Springer book series Foundations in Signal Processing, Communications and Networking. He has been involved as principal investigator in several research projects funded by the German Research Fund (DFG) and coordinated a German DFG priority program on Communications Over Interference Limited Networks. He is currently principal investigator of the 6G Future Lab of the Free State of Bavaria and the 6G-labs consortium of the German Federal Ministry of Education and Research.